Juvenile hormones direct primordial germ cell migration to the embryonic gonad

Barton, Lacy J[1,2], Sanny, Justina[1], Dawson, Emily P[1], Nouzova, Marcela[3,4], Noriega, Fernando Gabriel[3,5], Stadtfeld, Matthias[1,6], Lehmann, Ruth[1,7]

[1] Department of Cell Biology, Skirball Institute of Biomolecular Medicine, and Howard Hughes Medical Institute, NYU Grossman School of Medicine, NY, USA, 540 First Avenue, New York, NY 10016, USA

[2] Department of Neuroscience, Developmental and Regenerative Biology, The University of Texas at San Antonio, One UTSA Circle, San Antonio, TX, 78249, USA

[3] Department of Biological Sciences and Biomolecular Sciences Institute, Florida International University, 11200 SW 8th St, Miami, FL 33199, USA

[4] Institute of Parasitology, Biology Centre CAS, Ceske Budejovice, Czech Republic

[5] Department of Parasitology, University of South Bohemia, České Budějovice, 37005, Czech Republic

[6] Present: Department of Medicine, Weill Cornell Medicine, 413 E 69th St, New York, NY 10021, USA

[7] Present: Whitehead Institute and Department of Biology, MIT, 455 Main Street, Cambridge, MA 02142, USA

Highlights

- Juvenile hormones (JH) are necessary & sufficient for Primordial Germ Cell (PGC) migration.
- JH signaling acts directly in and around migrating PGCs prior to its endocrine function.
- Compensatory feedback sensitive to JH receptor function maintains JH homeostasis.
- JH-like retinoic acids may have similar roles during mammalian germ cell migration.

Summary

Germ cells are essential to sexual reproduction. Across the animal kingdom, extracellular signaling isoprenoids, such as retinoic acids (RAs) in vertebrates and juvenile hormones (JHs) in invertebrates, facilitate multiple processes in the germline lifecycle. Here we investigated the role of these potent signaling molecules in embryonic germ cell migration, using JHs in *Drosophila melanogaster* as a model system. In contrast to their established endocrine roles during larval and adult germline development, we found that JH signaling acts locally during embryonic development. Using an *in vivo* biosensor, we found JH signaling is first active near primordial germ cells (PGCs) as they migrate to the developing somatic gonad. Through *in vivo* and *in vitro* assays, we found that JHs are both necessary and sufficient for PGC migration. Analysis into the mechanisms of this newly uncovered paracrine JH function revealed that PGC migration was compromised when JHs were reduced or increased, suggesting that specific titers or spatiotemporal JH dynamics are required for robust PGC colonization to the gonad. Compromised PGC migration can impair fertility and cause germ cell tumors in many species, including humans. In mammals, retinoids, a JH-related family of signaling isoprenoids, has many roles in development and reproduction. We found that retinoic acid, like JH, was sufficient to impact PGC migration *in vitro*. Together, our study reveals a previously unanticipated role of isoprenoids as local effectors of pre-gonadal PGC development and suggests a broadly shared mechanism in PGC migration.

Key words: primordial germ cells, cell migration, gonad, germline, mevalonate pathway, juvenile hormone, retinoids

Introduction

In sexually reproducing species, the germline links one generation to the next. Given the importance to individuals, societies, and species, understanding how germ cells are set aside, develop, and protected until undergoing gametogenesis to yield sperm and egg has been the focus of intense efforts. Through recent advances in single-cell 'omics and *in vitro* derivation of primordial germ cell (PGC)-like cells from induced pluripotent stem cells, we have gained substantial insights into the molecular programs intrinsically required for germ cell specification and development. However, the yield and gamete quality of *in vitro* derivation approaches falls far short of what is observed *in vivo*[1]. This quality gap suggests that we are failing to recapitulate key aspects of germline development. One critical component not yet replicated *in vitro*, nor fully understood *in vivo*, is how germline development is exquisitely coordinated in space and time during embryogenesis by surrounding somatic cells.

Somatic cells coordinate germ cell development and gametogenesis through small, secreted molecules such as steroid hormones and signaling lipids. These potent molecules have multifaceted impacts on reproduction across the animal kingdom. In vertebrate animals, key reproductive small molecules include steroid hormones (i.e., estrogen and testosterone) that are synthesized from cholesterol, and paracrine retinoic acids (RAs), that are derived from carotenoids, a subfamily of isoprenoids. Animals lack the ability to synthesize carotenoids and thus obtain these critical molecules from their diet. Despite differences in biosynthetic origins and structures, invertebrate animals also use steroids and isoprenoids to facilitate many aspects of germline development and reproduction. In *Drosophila*, the steroid hormone, ecdysone, regulates germline stem cell homeostasis, niche development, yolk uptake, and the migratory behavior of certain ovarian somatic cell types[2-5]. The RA-like isoprenoids, Juvenile hormones, have profound impacts on reproduction. For example, methyl farnesoate is a key sex determination molecule in some crustaceans[6]. In many insects, JHs act as gonadotropins, with essential roles in vitellogenesis[7,8]. Recent work in *Drosophila* have revealed that JHs also regulate germline stem cell number and reproductive diapause[9,10].

While much is known about how steroid hormones mechanistically shepherd the germline lifecycle, how signaling isoprenoids regulate the germline lifecycle is much less understood. Given the complexity surrounding RAs in germline biology, insights can be gleaned from JHs. These potent sesquiterpenoids, derived from the mevalonate pathway[11], are best known for their influence on juvenile development[12]. They include, among others, JH III, JH III bisepoxide

105 (JHB_3), and methyl farnesoate (**Fig 1a**). As signaling molecules, JHs bind to a basic helix-loop
106 helix/Per-ARNT-SIM (bHLH-PAS) receptor, which in *Drosophila* is encoded by two paralogous
107 genes, *Methoprene-tolerant* (*Met*) and *germ cell-expressed bHLH-PAS* (*gce*)[13-15]. Upon ligand
108 binding, these receptors regulate gene expression together with the co-activator Taiman[16]. In
109 contrast to paracrine acting RAs, JHs act hormonally such that JH is synthesized in the corpus
110 allatum (CA), a neuroendocrine gland, and released into the circulatory system (**Fig 1a**). JH
111 production is driven by Juvenile hormone acid methyltransferase (Jhamt), which is expressed in
112 the CA as soon as this gland forms at the end of embryogenesis[17]. Curiously, a burst of *jhamt*
113 expression has also been observed in the trunk mesoderm during mid-embryogenesis, well
114 before the specification of the CA precursors[17], leaving open the possibility that JHs have
115 additional, non-endocrine roles.
116
117 Mesodermal *jhamt* expression coincides with the PGC migration stage of reproductive
118 development. In many species, newly specified PGCs are internalized during gastrulation and
119 then must migrate within the mesoderm toward the developing gonad to generate the germline
120 pool. In some mammals, including humans, extragonadal PGCs that fail to reach the gonad can
121 cause germ cell tumors[18]. To investigate the role of JHs during PGC migration, we first
122 generated an *in vivo* JH sensor and found that JH signaling was first active proximal to *jhamt*
123 expression and surrounding migratory PGCs. New *jhamt* mutants lacking the methyltransferase
124 domain compromised JH synthesis and caused a failure of PGCs reaching the gonad. A similar
125 defect in gonad colonization had previously been described in animals lacking HMG Coenzyme
126 A reductase (Hmgcr)[19], the rate-limiting enzyme of the mevalonate pathway upstream of Jhamt
127 in JH synthesis[11]. Consistent with Hmgcr and Jhamt being part of the same synthetic cascade,
128 we found that *jhamt* and *Hmgcr* genetically interact to facilitate PGC migration and that JH, like
129 Hmgcr, is both necessary and sufficient for PGC migration. Our further investigations into the
130 function of JH receptors in the embryo revealed a feedback mechanism necessary to maintain
131 JH homeostasis critical for PGC migration. Together, our studies uncovered a new requirement
132 for JH signaling in embryonic reproductive development. Studies in mice demonstrated that, like
133 JHs, genes critical to RA synthesis are expressed in the bipotential gonad during PGC
134 development PGC development[20-22]. However, despite shared expression of genes involved in
135 reproductive isoprenoids in vertebrate and invertebrate species, a role for isoprenoid signaling
136 during the PGC migration has not been described. Here we demonstrate that RA is sufficient to
137 induce migration of both *Drosophila* and mouse embryonic germ cells, suggesting this newly

138 identified role for secreted isoprenoids on early germline development may be broadly shared
139 across invertebrate and vertebrate species.
140
141
142
143 **Results**
144
145 Juvenile hormone signaling is active in the embryonic mesoderm during PGC development
146
147 Juvenile hormone production is driven by Juvenile hormone acid methyltransferase (Jhamt).
148 Jhamt is specifically expressed in the corpus allatum (CA), as soon as this JH-producing
149 endocrine gland develops in late embryogenesis[17]. Curiously, in *Drosophila jhamt* mRNA is also
150 detected during mid-embryogenesis in the trunk mesoderm, before specification and migration
151 of CA precursors[17]. Using dual-label fluorescent *in situ* hybridization for mRNAs encoding Jhamt
152 and the germ cell factor, Nanos, we investigated where *jhamt* is expressed relative to PGCs.
153 Consistent with previous work[17], we observed *jhamt* expression in the mesoderm from
154 embryonic Stage 10 (~4 hours after fertilization), continuing through Stage 13 (~11 hours after
155 fertilization) (**Fig 1b**). At this stage in embryogenesis, PGCs exit the endoderm and sort into two
156 lateral populations as they migrate within the mesoderm toward the somatic gonadal precursors
157 (**Fig 1c**). This *jhamt* expression pattern suggested that JH synthesis may occur prior to CA
158 formation and be involved in embryonic germline development.
159
160 To determine whether mesodermal *jhamt* mRNA leads to functional JH production during
161 *Drosophila* embryogenesis, we generated an *in vivo* JH sensor. We placed *eGFP* downstream
162 of eight tandem copies of a JH response element (JHRE) from the *early trypsin* gene of *Aedes*
163 *aegypti*[15,23], which was previously shown to robustly and specifically responds to JH *in vitro*[15]
164 (**Fig 1d** and **Supp Fig 1a**). To test the responsiveness of this biosensor to JH *in vivo*, we fed
165 second instar larvae the JH mimic, methoprene, and measured mRNA levels of *GFP* and the
166 canonical JH signaling transcriptional target, *Krüppel homolog 1* (*Kr-h1*), by real-time-qPCR 24
167 hours later. We found that *Kr-h1* and *GFP* mRNA levels increased ~two-fold and seven-fold
168 respectively in *JHRE-GFP* larvae fed methoprene (**Fig 1d**). To determine whether this induction
169 by methoprene required JH signaling, we generated animals carrying the JHRE sensor but
170 lacking the JH receptors, Methoprene-tolerant (Met) and Germ cell-expressed bHLH-PAS (gce).
171 We found that methoprene did not increase expression of either *Kr-h1* or *GFP* mRNA in *Met,*

172 *gce; JHRE-eGFP* mutant animals (**Fig 1d**). Together, these data indicate that this new JH
173 sensor faithfully responds to JH signaling *in vivo*.
174
175 With this *in vivo* JH sensor, we next investigated if and where JH signaling is active during
176 embryonic germline development. We stained *JHRE-GFP* embryos with antibodies against GFP
177 and the germ cell-specific RNA helicase, Vasa. GFP signal was first detected in Stage 10
178 embryos in two locations: in bilateral clusters in the anterior portion of the embryo and in
179 bilateral strips of the mesoderm of the posterior germband (**Fig 1e, f**). The anterior signal was
180 still detected in *Met, gce* mutant embryos carrying the JH biosensor, but the germband signal
181 was absent (**Fig 1e**). To explore whether this difference is due to non-specific, receptor-
182 independent transgene activation, we analyzed animals carrying a JH sensor transgene in
183 which the Met/gce binding motif was mutated (**Supp Fig 1a**)[15]. Anterior GFP was still present in
184 animals with the mutated biosensor; further investigation revealed that this non-JH-specific GFP
185 signal localized to hemocytes (**Supp Fig 1b-c**). Importantly, the mesodermal signal was not
186 detected in embryos carrying the JH biosensor with mutated receptor binding motifs, nor when
187 the functional biosensor JHRE-eGFP was tested in *Met, gce* receptor mutants. Thus, the
188 mesodermal signal is due to JH-mediated receptor activation and reflects JH signaling. We
189 found that this specific JH sensitive response began at Stage 10 in the mesoderm, when PGCs
190 enter this tissue from the endoderm. JH signaling continued to localize in and near PGCs as
191 they colonized the gonad (**Fig 1e, Supp 1c**). Together, these data demonstrate that JH
192 signaling is active near the mesodermal *jhamt* expression zone and surrounds migratory PGCs
193 during mid-embryogenesis.
194
195
196 <u>Juvenile hormones are required for migrating PGCs to reach the somatic gonad</u>
197
198 To determine whether the newly identified embryonic JH signaling supports early PGC
199 development, we generated new mutant *jhamt* alleles. Using CRISPR editing, 15 *jhamt* alleles
200 were generated, two of which carried a premature stop codon at amino acid 46, whereas the
201 remaining 13 carried a premature stop codon at amino acid 54 (**Supp Fig 2**). All new alleles
202 caused a deletion of the methyl transferase domain central to Jhamt-mediated JH biosynthesis
203 (**Fig 2a**). To avoid confounding effects from second site mutations, phenotypic analyses carried
204 out in this study use the newly generated *jhamt* lines in heteroallelic combinations or *in trans* to
205 an independently generated small deficiency lacking the entire *jhamt* locus (**Supp Table 1**). To

206 verify that Jhamt function was compromised, titers of two JHs in *Drosophila*, JH III and JHB_3,
207 were directly quantified by liquid chromatography-tandem mass spectrometry[24]. We found that
208 JH III titers were reduced 50% and JHB_3 titers were reduced >90% in larvae possessing our
209 newly generated alleles (**Fig 2b**). These results are consistent with previous observations
210 showing that JHs were still detected in animals lacking the entire *jhamt* locus[25], suggesting the
211 *Drosophila* genome may contain a second, yet obscure, methyltransferase capable of JH
212 synthesis[26,27]. To attest the degree by which JH function was compromised, we measured
213 female fecundity. Consistent with previous reports[25], the number of eggs laid per day was
214 significantly reduced in females carrying our new *jhamt* mutant alleles (**Fig 2c**). Together, these
215 data suggest that the newly generated *jhamt* mutants significantly affected JH production and
216 display JH loss of function phenotypes.
217
218 With new genetic tools, we next compared PGC development in wildtype and *jhamt* mutant
219 embryos. The first detectable germline defect in *jhamt* mutant embryos was an increased
220 number of PGCs that failed to reach the gonad at Stage 14, when PGC normally have
221 completed their migration to the somatic gonad (**Fig 2d)**. Animals lacking zygotic Jhamt had
222 significantly more extragonadal PGCs than wildtype animals (**Fig 2e**). This phenotype was
223 rescued when *jhamt* was zygotically expressed with a broad *Tub-GAL4* driver (**Fig 2e**). These
224 data indicate that *jhamt* expressed in somatic cells facilitates PGC migration to the developing
225 somatic gonad.
226
227 The *jhamt* mutant PGC phenotype was similar to that of embryos lacking HMG-CoA reductase
228 (Hmgcr), the rate-limiting enzyme in the mevalonate pathway (**Fig 2d** and **e**)[19]. In *Drosophila*,
229 Hmgcr was shown to have a striking, instructive effect on PGC migration: in *Hmgcr* mutant
230 embryos PGCs failed to reach the gonad and when mis-expressed, elevated *Hmgcr* expression
231 alone mislocalized PGCs to the location of ectopic expression (**Fig 2f** and **Supp Fig 2a,**
232 **b)**[19,28,29]. Our observation that *jhamt* mutants phenocopied *Hmgcr* mutants is consistent with
233 previous reports that Hmgcr is required for JH synthesis and genetically interacts with *jhamt* in
234 the context of animal development[25]. To determine whether Jhamt functions downstream of
235 Hmgcr in embryonic PGC migration, we tested for genetic interaction in two ways. First, we
236 measured the effect of genetic *Hmgcr* reduction in sensitized *jhamt* heterozygous animals and
237 found that significantly more PGCs failed to reach the gonad in $jhamt^{+/-}$; $Hmgcr^{+/-}$ heterozygous
238 embryos than embryos heterozygous for *jhamt* alone (**Fig 2e**). Second, we tested whether
239 genetic reduction of Jhamt can suppress the ability of ectopic *Hmgcr* expression to misdirect

240 PGCs. Indeed, loss of one wildtype *jhamt* copy significantly reduced the number of PGCs
241 misdirected by GAL4/UAS-mediated expression of *Hmgcr* (**Fig 2f**). Together, these data
242 suggest that Jhamt functions downstream of Hmgcr to facilitate PGC migration to the somatic
243 gonad.
244
245
246 Juvenile hormone is sufficient for PGC migration
247
248 Hmgcr is sufficient to misdirect migrating PGC to many tissues, even tissues far from the normal
249 migratory path such as the central nervous system (**Fig 3a** and **Supp Fig 3a**)[19,28,29]. To
250 determine whether, like *Hmgcr*, *jhamt* expression is sufficient for PGC migration *in vivo*, we
251 ectopically expressed *jhamt* mRNA using the GAL4/UAS system. We found that neuronal *Elav-*
252 *GAL4* driven *jhamt* expression led to modest, yet significant, increase in PGCs inappropriately
253 near neuronal Elav-positive cells (**Fig 3b**). We even found some PGCs localized in the central
254 nervous system after neuronal *jhamt* expression (**Fig 3a**). Yet overall, significantly fewer PGCs
255 were misdirected by ectopic *jhamt* compared to ectopic *Hmgcr* driven by the same *Elav-GAL4*
256 transgene (**Fig 3b**). Moreover, ectopic *jhamt* expression was insufficient to drive PGCs to
257 inappropriate locations when *UAS-jhamt* was induced by the endodermal driver, *48Y-GAL4*, or
258 the pan-mesodermal drivers, *twist-GAL4* and *24B-GAL4*, even though ectopic *Hmgcr*
259 expression with these GAL4 drivers significantly mislocalized PGCs (**Supp Fig 3b**). These data
260 show that Jhamt was sufficient to impact PGC migration *in vivo* in at least one, but not all,
261 tissues, suggesting that other pathway components may be limiting.
262
263 Hmgcr and Jhamt are both required for JH biosynthesis. There are at least two possible
264 explanations for the difference by which ectopic expression of *jhamt* and Hmgcr was sufficient to
265 attract PGCs *in vivo* (**Supp Fig 3b**). Hmgcr may direct PGCs through production of JH and non-
266 JH signals. Indeed, Hmgcr is required for the synthesis of many molecules and post-
267 translational protein modifications[29]. Alternatively, *jhamt* expression may not be sufficient in
268 every tissue due to a lack of precursors derived from the upstream mevalonate pathway.
269 Indeed, Hmgcr is the rate-limiting enzyme in the mevalonate pathway and it's expression is
270 spatially restricted during mid-embryogenesis[19]. To assess the role of JH directly, we turned to
271 an *in vitro* transwell migration assay, in which *Drosophila* PGCs were obtained from whole
272 embryos, enriched by fluorescence-activated cell sorting (FACS), and placed on a porous filter
273 above media (**Fig 3c**). Previous work showed that PGCs will translocate in response to serum-

free culture media conditioned with Kc167 or S2 embryonic *Drosophila* cells[30] (**Fig 3d**). To explore the impact of JH on PGC migration in this *in vitro* migration assay, we knocked down *jhamt* mRNA in Kc167 cells using two, independent dsRNAs (**Supp Table 3**), collected conditioned media, and measured PGC translocation. Like Hmgcr depletion[30], significantly fewer PGCs translocated in response to media that was conditioned by *jhamt*-depleted Kc167 cells compared to control conditioned media (**Fig 3d**). To verify that reduced PGC translocation was not due to fewer Kc167 cells conditioning the media, we quantified Kc167 cell number and found that *jhamt* depletion had no effect (**Supp Fig 3b**). These data indicated that Jhamt, produced in somatic cells, facilitated PGC migration *in vitro*.

We next asked whether JHs are sufficient for PGC migration. To this end, FACS-enriched PGCs were placed on the transwell filter above serum-free, unconditioned culture media supplemented with commercially available JH III with 1% BSA as a non-specific carrier protein. We found that PGCs translocated in response to JH III, with a positive correlation with JH concentration except at the highest JH concentration tested (**Fig 3e**). To test the specificity of this response, we subjected PGCs to the JH III analogue and insecticide, Methoprene, and found that PGCs translocated in response to Methoprene at levels comparable to JH III (**Fig 3f**). Together, these data demonstrated that JHs were sufficient to induce or direct PGC migration.

<u>Compensatory feedback maintains JH homeostasis in *Drosophila melanogaster*</u>

Our findings suggested that JHs originating from the somatic mesoderm direct PGC migration to the somatic gonad. We next investigated the mechanisms by which PGCs respond to JHs. JH signaling response canonically involves JHs binding to the Met/Gce receptor, which then associates with a co-activator Taiman to influence transcription of target genes (**Fig 1a**)[15]. To determine whether the JH receptors are required for PGC migration, we analyzed embryos mutant for the two, partially redundant, JH receptors[14,15]. As existing *Met, gce* double mutant strains die during metamorphosis[14], to test the maternal and zygotic contributions of Met/Gce we generated new Met^{1}, $gce^{Mi02742}$ double mutants. In $gce^{Mi02742}$, *gce* mRNA is reduced by more than 90% (**Fig 4a** and **b**) and Met^{1} carries a point mutation that renders *Drosophila* 33-fold more resistant to lethality inflicted by methoprene[31]. This strain was crossed with Met^{27}, $gce^{2.5k}$ heterozygous females. Even under non-crowding conditions, only ~5% of the expected class of heteroallelic *Met, gce* double mutant animals eclosed. As expected[14,32], the fecundity of these

308 escaper *Met, gce* females was significantly reduced (**Fig 4c**), but nevertheless, allowed us to
309 analyze Met and Gce requirements in PGC development.
310
311 To investigate PGC response requirements, we stained maternally and zygotically *Met, gce*
312 mutant embryos for Vasa and DAPI. Embryos lacking either maternal or zygotic Met and gce
313 showed a moderate loss of PGCs relative to wildtype controls at the end of migration (**Fig 4d**).
314 However, we observed a significant increase in the number of extragonadal PGCs in embryos
315 lacking both maternal and zygotic Met and gce (**Fig 4d**). Because PGCs primarily rely on
316 maternally deposited mRNAs during migration[33], the additive effect of maternal and zygotic loss
317 suggests either an early somatic requirement or a late PGC requirement for Met/gce. To test for
318 a link between JH receptors and Hmgcr, we next asked whether Met/Gce suppressed the ability
319 of PGCs to respond to Hmgcr. For this experiment, we took advantage of our observation that
320 ectopic *Hmgcr* expression in the endoderm trapped 50-80% of PGCs within the gut at Stage 10
321 (**Fig 4e**). To test whether loss of Met and Gce suppressed the ability of ectopic *Hmgcr*
322 expression to trap PGCs, we crossed wildtype or *Met, gce* double mutant females to males
323 containing *48Y-GAL4* and *UASt-Hmgcr* transgenes and quantified the percentage of PGCs
324 remaining in the gut after gonad colonization (**Fig 4e**). This experiment revealed a small, but
325 statistically significant, suppression of gut trapping in maternally *Met, gce* mutant PGCs (**Fig**
326 **4e**). Together, these data are consistent with a requirement for Met and Gce in PGC migration
327 to the gonad downstream of Hmgcr/JH signaling.
328
329 Canonical JH signaling leads to transcriptional changes of target genes. To determine whether
330 transcription is required for PGCs to respond to JHs, we returned to the *in vitro* migration assay,
331 where we inhibited transcription specifically in PGCs using the P-TEFb-associated CDK9
332 inhibitor, flavopiridol. As expected[34], flavopiridol rapidly and robustly inhibited transcription in
333 PGCs enriched by FACS (**Supp Fig 4**). We then subjected control and transcriptionally deficient
334 PGCs to conditioned media, serum-free media, or serum-free media containing JH III and found
335 that inhibition of transcription did not alter PGC translocation in response to any condition tested
336 (**Fig 4f**). These data suggest that the migratory response of PGCs to JH does not depend on
337 classical transcription-dependent JH receptor signaling.
338
339 We were surprised that PGC migration to the gonad was compromised in *Met, gce* mutant
340 animals *in vivo*, yet transcription was not required for JH-mediated PGC migration JHs *in vitro*.
341 However, we noticed that extragonadal PGCs in *Met, gce* mutant embryos were often located

342 centrally and anterior to the gonad, rather than posterior to the gonad as observed in *jhamt* and
343 *Hmgcr* mutant embryos (**Fig 2d** and **Fig 4d**). The central, anterior location of extragonadal
344 PGCs in *Met, gce* mutant embryos suggests that migration to the gonad may be compromised
345 at an earlier stage than in *jhamt* mutant embryos. One possible explanation is that altered JH
346 homeostasis within the embryos, rather than loss of JH signaling response in migrating PGCs,
347 were the cause of extragonadal PGCs in *Met, gce* mutants. To test this possibility, we measured
348 JH titers by quantitative mass spectrometry. Interestingly, we found that both JH III and JHB_3
349 titers were dramatically increased in *Met, gce* mutant animals relative to wildtype (**Fig 5a**). To
350 investigate how JH titers could be increased in *Met, gce* mutant animals, we measured *jhamt*
351 mRNA levels by real time-qPCR. We found increased *jhamt* mRNA levels in *Met, gce* mutants in
352 several life stages, including during mid-stage embryo embryogenesis (**Fig 5b** and **Supp Fig**
353 **5a**). Consistent with compromised JH-dependent transcriptional signaling, expression of the
354 target gene, *Kr-h1*, was not increased in *Met, gce* mutant animals (**Fig 5b**). These data
355 uncovered a compensatory feedback mechanism in *Drosophila melanogaster* by which JH
356 receptors mediate JH titer homeostasis. Importantly, this study suggests that PGC migration to
357 the gonad is compromised by either decreased or increased JH levels.
358
359
360 Isoprenoids in PGC migration
361
362 JHs belong to a broader class of secreted isoprenoids that have functions in reproduction
363 throughout the animal kingdom. Such molecules include methyl farnesoate, which has potent
364 impacts on sex differentiation in the crustaceans[6], and retinoic acids (RAs), which have
365 pleiotropic effects at many stages of vertebrate reproductive development and gametogenesis[35-
366 37]. Although the transcriptional receptors differ, they are promiscuous enough to bind to a broad
367 class of exogenous secreted isoprenoids and other small molecules[38]. To determine whether *in*
368 *vitro* cross-activation extends to PGC migration, we enriched *Drosophila* PGCs by FACS and
369 subjected them to JH III or two RA species, all-trans retinoic acid (ATRA) or 9-cis RA. Notably,
370 9-cis RA induced *Drosophila* germ cell translocation to levels comparable of JH III (**Fig 6a**).
371 These data show that RAs can induce *Drosophila* PGC migration, suggesting commonality in
372 response to this class of secreted isoprenoids.
373
374 Our studies revealed that the JH biosynthesis enzyme was present in the mesoderm near PGCs
375 as they migrated toward the developing somatic gonad during *Drosophila* embryogenesis.

376 Interestingly, the enzymes critical for RA biosynthesis are also expressed in the developing
377 bipotential somatic genital ridge of mouse embryos as germ cells are colonizing this tissue[21]. To
378 determine whether RAs may have a similar role in vertebrate germ cell development, we
379 adapted the *in vitro* transwell migration assay developed for *Drosophila* PGCs to mouse germ
380 cells. To this end, we obtained mouse germ cells by FACS from embryonic day E10.5 mice
381 carrying a germ cell-specific transgene (*Oct4ΔPE:GFP*) (**Supp Fig 6a**). At this stage in
382 reproductive development, mouse PGCs are completing their migration and beginning to
383 populate the bipotential somatic gonad. We exposed germ cells to fetal bovine serum in PGC
384 media as a positive control or serum-free PGC media as a negative control. Both ATRA and 9-
385 cis RA induced translocation of mouse embryonic germ cells to levels comparable to the known
386 mouse and zebrafish PGC chemoattractant, C-X-C Motif Chemokine Ligand (CXCL12) (also
387 called SDF1a) (**Fig 6b**)[39-41]. Although RAs can have a proliferative effect on mouse PGCs over
388 24-72 hours[42], we did not detect changes in total PGC number during our two-hour assay (**Supp**
389 **Fig 6b**). Therefore, the increased number of translocated PGCs was not due to RA-induced
390 proliferation. Together, these data suggest that the newly uncovered role of secreted
391 isoprenoids in early PGC migration and colonization to the somatic gonad may be broadly
392 shared among invertebrate and vertebrate species.
393
394
395
396 **Discussion**
397
398 Germ cells are shepherded through development and differentiation by surrounding somatic
399 cells, which provide hormones and other signaling molecules. Here, we demonstrated that
400 Juvenile Hormones (JHs), key gonadotropins in adult gametogenesis, functioned in embryonic
401 reproductive development. In the embryo, JH signaling was spatially restricted and enriched
402 around PGCs as they migrated to the somatic gonad. We found that JHs were necessary *in vivo*
403 and sufficient *in vitro* for PGC migration. Together, these studies significantly expanded our
404 understanding of the scope, functions, and mechanisms by which JHs support the germline
405 lifecycle.
406
407
408
409

410 JH signaling is active during embryogenesis prior to endocrine gland formation in *Drosophila*
411
412 The study of JH biology has largely focused on endocrine production in juvenile and adult
413 animals, particularly for insects that undergo a complete metamorphosis, like *Drosophila*. In
414 juvenile and adult animals, JHs are produced in the CA endocrine gland. CA precursors are first
415 distinguishable at Stage 13 and migrate dorsally to form the ring gland at Stage 15[43,44]. Through
416 the generation of an *in vivo* JH sensor, we provide evidence that JH signaling is active in
417 *Drosophila* embryos starting at Stage 10 (**Fig 1e** and **f**). Our data are consistent with a burst of
418 *Kr-h1* expression in 8-12 hr old embryos[45,46] and with recent reports of non-CA *jhamt* expression
419 in gut cells[47]. Combined, these studies show that sources of these important hormones exist
420 outside of the CA. Three species of biologically active JHs detected in *Drosophila* are proven
421 agonist ligands of Gce[25,48], yet whether these forms are temporally and functionally distinct *in*
422 *vivo* are unknown. The discovery of embryonic JH activity in the genetically tractable *Drosophila*
423 embryo and in an *in vitro* migration assay provide a unique opportunity to explore JH species-
424 specific functions.
425
426
427 JH signaling is paracrine during mid-embryogenesis
428
429 We observed JH activity near mesodermal expression of JH-producing enzyme Jhamt (**Fig 1b,**
430 **e, f**). This observation suggests that JH signaling is paracrine during embryogenesis. Paracrine
431 signaling mechanisms are consistent with reports that adult gut cells exhibit local JH signaling[49]
432 and that ectopic *Hmgcr* expression influences PGC migration within a ~50um zone[28]. How JH
433 signaling response is spatially restricted has yet to be understood, but one possibility is that JH
434 transport or diffusion is limited by the dense extracellular environment of the embryo.
435 Alternatively, JH signaling may be restricted by the spatio-temporal expression of enzymes that
436 synthesize or degrade JHs or be restricted to cells that possess all required factors in the
437 transcriptional signaling cascade. Whether all co-factors are present in all somatic cells during
438 mid-embryogenesis is unknown, however the core JH transcription factors, *Met, gce* and *taiman*
439 mRNAs are maternally loaded into the early embryo[50-53]. Whether JH binding proteins, which
440 facilitate JH circulation in whole juvenile and adult insects, are required for embryonic JH
441 signaling is unknown. The highly dynamic, well-characterized, and pre-circulatory features of
442 mid-embryogenesis can be leveraged to understand the mechanisms of paracrine JH signaling.
443

444

445 JH signaling ensures migrating PGCs reach the somatic gonad

446

447 Embryonic JH signaling is enriched in the trunk mesoderm as PGCs migrate in this tissue
448 toward the somatic gonad (**Fig 1c, e, f**). We found that JH biosynthesis enzymes are necessary
449 for efficient gonad colonization *in vivo* and JHs are sufficient for PGC migration *in vitro* (**Fig 2**
450 and **Fig 3**). While JHs have many functions in reproduction, our findings demonstrate that JH
451 activity impacts germline development far earlier than previously appreciated. Moreover, a role
452 for JHs in cell migration had not been reported to our knowledge. In contrast, ecdysone, the
453 steroid hormone controlled, in part, by JHs[54], regulates the migration of many somatic ovarian
454 cell types, including swarm cells during juvenile ovarian development[3] and border cells during
455 adult gametogenesis[4]. Given the antagonistic relationship between the steroid ecdysone and
456 the isoprenoid JHs[54], it remains possible that JHs also prevent ecdysone-mediated processes
457 while germ cells colonize the gonad. Such regulation by JHs may have been obscured by the
458 relatively high degree of genetic redundancy throughout the JH biosynthetic, degradative, and
459 signaling response cascades in the *Drosophila* genome[15,25,26]. The findings described here
460 provide an opportunity to understand the relationship between steroid hormones and JH/retinoid
461 signaling molecules. Indeed, antagonism between these two classes of signaling molecules are
462 observed in multiple tissue contexts throughout the animal kingdom[54,55].

463

464 Our findings that JHs impact PGC migration opens many questions. Do JHs regulate PGC
465 directionality or motility? What signaling events are required for migrating PGCs to respond to
466 JHs? Classic JH signaling involves receptor-mediated transcription. In contrast, we find that
467 transcription is not required in PGCs for migrational response to JHs *in vitro* (**Fig 4f**). Our finding
468 is consistent with the observation that PGCs respond to ectopic Hmgcr prior to full activation of
469 their zygotic genome (**Fig 4e**) and that migrating PGCs must rapidly respond to environmental
470 changes. Rapid responses to JHs during ovarian follicle development has been observed for
471 decades[56-59], however the mechanisms remain elusive. Both receptor tyrosine kinases and G
472 protein-coupled receptors (GPCRs) have been implicated in rapid responses to JHs[60,61]. A
473 requirement for GPCRs is consistent with our observations that migratory response of
474 *Drosophila* PGCs is attenuated at the highest dose of JHs *in vitro* (**Fig 3e**) and compromised
475 when JH titers are elevated *in vivo* (**Fig 4d** and **5a**), a characteristic feature of GPCR
476 desensitization. Identification of a plasma membrane receptor capable of mediating a rapid

477 response to JHs and related molecules during early PGC development will be an exciting area
478 of future exploration.
479
480 Signaling responses to JHs usually involve DNA-binding receptors that induce transcription. We
481 found that the *Drosophila melanogaster* JH receptors, Met/Gce, are required for PGCs to
482 efficiently migrate to the gonad (**Fig 4d**) downstream of Hmgcr (**Fig 4e**). However, genetic
483 suppression of Hmgcr-mediated trapping was mild and the location of extragonadal *Met, gce*
484 PGCs differs compared to embryos lacking the JH biosynthesis enzymes. In the absence of
485 Jhamt and Hmgcr, extragonadal PGCs are often found lateral and posterior to the gonads,
486 whereas extragonadal *Met, gce* PGCs are found medially and anterior to the gonads (**Fig 2d**
487 and **Fig 4d**). While anterior extragonadal PGCs could result from failing to stop migrating at the
488 target gonad, the medial localization and frequent endodermal association of *Met, gce* PGCs
489 suggests that migration is compromised earlier than in *jhamt* mutants. There are a few possible
490 explanations for this surprising observation. First, JH signaling may be more compromised
491 earlier and stronger in *Met, gce* mutants than in *jhamt* mutants. Indeed, loss of *jhamt* does not
492 completely abolish JH titers (**Fig 2b**), as has been reported previously[25]. Second, JH signaling
493 may be required maternally as JHs are maternally provided into eggs in some species[62].
494 However, it should be noted that zygotic loss of Jhamt and Hmgcr is sufficient to compromise
495 PGC migration (**Fig 2d**)[19]. Third, migration may be compromised in *Met, gce* mutant animals
496 because JH titers are increased (**Fig 5a**). Future work will be needed to elucidate precisely how
497 Met and/or Gce are required for PGC development. Yet, our findings suggest that either a
498 specific titer or spatial arrangement of JHs are required for PGCs to efficiently populate the
499 somatic gonad. How PGCs respond to finely tuned JH availability will be an interesting area of
500 future exploration.
501
502
503 <u>Discovery of a compensatory feedback loop that maintains JH homeostasis</u>
504
505 Animals carrying mutations in the JH receptors exhibit dramatically high JH titers (**Fig 5a**).
506 Elevated JH titers coincided with increased *jhamt* mRNA levels at multiple *Drosophila* life stages
507 (**Fig 5a**, **b** and **Supp Fig 5a**), suggesting that constitutive feedback ensures stage-appropriate
508 JH titers upon genetic perturbations. The mechanism of this compensatory loop is not known,
509 however Met, Ecdysone Receptor (EcR), and their shared co-factor, Taiman, binding has been
510 detected ~1kb upstream of the *jhamt* transcription start site[63] (**Supp Fig 5b**). Thus, a simple

511 feedback mechanism may involve either Met/Gce-Tai repression or EcR-Tai activation of *jhamt*
512 transcription. Indeed, reduced *Kr-h1* mRNA observed in *Met, gce* animals (**Fig 5b**) may lead to
513 the upregulation of EcR-dependent signaling as ecdysone biosynthesis genes are repressed by
514 Kr-h1[64,65]. For these studies, we used the Met^{1} allele, which encodes a point mutation in a highly
515 conserved position of the PAS-A domain and the Met^{27} allele, which strongly reduces *Met*
516 mRNA but the open reading frame appears wildtype (Marek Jindra, personal communication).
517 Both Met^{1} and Met^{27} mutant animals have dramatically increased tolerance to methoprene[31].
518 However, in our hands, adult escapers could only be obtained in heteroallelic $Met^{1/27}$, $gce^{Mi/2.5k}$
519 combination. Even under sparse conditions, homoallelic $Met^{27/27}$, $gce^{2.5k/2.5k}$ were not observed,
520 suggesting either the presence of a second site lethal mutation in the Met^{27}, $gce^{2.5k}$ genetic
521 background or that $Met^{1/27}$, $gce^{Mi/2.5k}$ animals have enough JH signaling to support development
522 through increased JH titers. The later explanation is more likely because UAS-driven *Met* or *gce*
523 can rescue $Met^{27/27}$, $gce^{2.5k/2.5k}$ lethality[15]. Moving forward, it will be important to expand the
524 experimental tools available to dissect this robust signaling pathway.
525
526
527 <u>New animal model to understand isoprenoid signaling in embryonic reproductive development</u>
528
529 We found that JH ensures that migrating PGCs reach the somatic gonad of the *Drosophila*
530 embryo. In contrast to systemic endocrine signaling in other life stages, our findings
531 demonstrate that during mid-embryogenesis, JH signaling is active near mesodermal
532 expression of the key JH biosynthesis enzyme, Jhamt. This local, paracrine signaling is similar
533 to how retinoic acids (RAs) act within vertebrate species. Indeed, the bioavailability of RAs and
534 JHs during analogous stages of germ cell development is strikingly similar between mice and
535 *Drosophila*, respectively[20-22,66]. RAs impact the migration of many cell types. Although most
536 investigations into the role of RAs in cell migration have focused on transcriptional upregulation
537 of chemokines or their receptors[67,68], evidence for transcription-independent functions of RAs is
538 an emerging field[69]. RAs facilitate axon guidance in *Xenopus laevis*[70], and in snails through non-
539 transcriptional mechanisms involving calcium flux, Rho GTPases and G proteins[71-74]. The many
540 similarities in structure, function, and periodic presence throughout the germline lifecycle
541 support the hypothesis that the isoprenoid signaling molecules, JHs and RAs, are functionally
542 analogous in reproductive development across the animal kingdom. We assert that *Drosophila*
543 can be a powerful genetic model to understand the primary functions and molecular
544 mechanisms by which environmentally pervasive isoprenoids impact reproductive development.

Such investigations will increase our understanding of how germ cell development is supported by surrounding somatic cells, both endogenously and through *in vitro* gametogenesis technologies.

Acknowledgements

We thank Marek Jindra and Ryusuke Niwa for reagents and valuable discussions, and Peter Nicholls and David Page for instructive discussions on mammalian reproductive development and assay development. We are grateful to Alexey A Soshnev for graphical designs, Cesar Ramirez and Francisco Fernandez-Lima for assistance with mass spectrometry. We are especially grateful to Rebecca Spokony, Jessica Treisman, Pamela K Geyer, and Toby Lieber for valuable advice and insightful discussions, as well as all members of the Lehmann laboratory for valuable input. Stocks obtained from the Bloomington Drosophila Stock Center (NIH P400D018537) were used in this study. In addition, several monoclonal antibodies used in this study were obtained from the Developmental Studies Hybridoma Bank, created by the NICHD of the NIH and maintained at The University of Iowa, Department of Biology, Iowa City, IA. We, like most users of the *Drosophila* model organism, could not have done this work without the efforts of the FlyBase Consortium (supported by NHGRI #U41HG000739 and #S454486, NSF #2039324, MRC #MR/W024233/1)[75]. We also thank the NYULMC Core Cytometry Facility, which is partially funded by NIH/NCI P30CA016087. This work was supported by a Damon Runyon Cancer Research Foundation postdoctoral fellowship from the William Raveis Charitable Fund (DRG2235-15, L.J.B), an NIH Pathway to Independence award (K99 and R00 HD097306, L.J.B.), an NIH-NIAID R21 award (R21AI167849, F.G.N), and project 22-21244S from the Czech Science Foundation, Czech Republic to MN and an NIH MERIT award (R37HD41900, R.L). RL was a HHMI investigator.

Author Contributions

Conceptualization: LJB, RL; Experimentation: LJB, JS, EPD MN, FGN, MS; Analysis: LJB, MN, FGN; Writing: LJB, RL; Funding Acquisition: LJB, RL; Supervision: LJB, MS, RL

Declaration of Interest

The authors declare no competing interest

STAR Methods

Animal Maintenance

Drosophila melanogaster were raised on medium containing 1.5% yeast, 3.6% molasses, 3.6% cornmeal, 0.112% Tegosept, 1.12% alcohol and 0.38% propionic acid. For embryo collections, apple juice plates contained 25% apple juice, 2.5% sucrose, 2.25% bactoagar, 0.15% Tegosept. Animals were kept at 25°C for all experiments. Fly strains used in this study are listed in Supplementary Table 1.

Mice expressing a germ cell-specific *Oct4ΔPE:GFP* transgene[76] (B6; CBA-Tg(Pou5f1-EGFP)2Mnn/J) were obtained from Jackson Laboratory (#004654, Bar Harbor, ME, USA). All protocols were approved by the NYU Institutional Animal Care and Use Committee.

Generation and validation of the P [*JHRE-GFP, w+]* transgenic biosensor

Eight copies of the wildtype JH response element (JHRE) from the *early trypsin* gene from *Aedes aegypti*[23], or eight tandem copies of the mutant JHRE (Supp Fig 1), were excised from *pGL4.17* vectors provided by Jindra Marek. JHREs were inserted upstream of the minimal *hsp70b* promoter and *eGFP* coding sequence of pS3aG transformation vector (Addgene #31171) containing an *attb* for site-specific integration. JHRE::GFP sensor constructs were integrated into *y+, attP2* at cytological position 68A4 sites by Bestgene.

To validate the JH sensor, transgenes were placed in met^{1}, gce^{MI} mutant background. Embryonic GFP signal was measured by immunohistochemistry. To measure JH responsiveness, first instar larvae were placed in food containing 1.6µg of Methoprene per gram of food [77], or ethanol as a control for 24 hours. *GFP* and *Kr-h1* mRNA was measured in whole second instar larvae by qPCR using primers in Table 3 (Fig 1 and Supp Fig 1).

Generation of *jhamt* alleles

The CRISPR guide CCTGGATGTGGTTCAGGATCT was cloned into pU6-2 gRNA vector (DGRC #1363) and injected into embryos into a stock derived from BL51324 carrying w^{1118} ;; *PBacy[mDint2]=vas-cas9VK00027* by Bestgene. Of 29 fertile founders, 87 F1 crosses were set up and screened for *jhamt* mutations by PCR amplification and Sanger sequencing using primers listed in Table 3. Of 48 F1 lines screened, 13 lines were obtained wherein small indels created a frame shift just before the methyltransferase domain, which starts at amino acid 40, leading to a stop codon just downstream, two lines at amino acid 46 (12F1 and 12F2) and the remaining lines at amino acid 54 (1F1, 1F2, 4F1, 4F3, 6F3, 7F2, 7F3, 8F1, 8F2, 12F3, 14M2, 14M3). The effect of new *jhamt* mutations on JH III and JHB_3 titers were quantified in third instar larval hemolymph.

623
624 Embryo Immunofluorescence
625 Prior to embryo collection, young parental strains (less than 5 days old) were mated in vials for
626 one day before transferring to embryo collection cages containing apple juice plates and wet
627 yeast. Embryos were dechorionated in 50% bleach for three minutes, rinsed with water and
628 fixed in a scintillation vial containing 2ml of 4% formaldehyde in PBS and 8ml of heptane.
629 Embryos were fixed for 20 minutes on a shaker. To remove the vitelline membrane,
630 formaldehyde was removed from the scintillation vial and 10ml methanol was added, followed
631 by one minute of vigorous shaking by hand. Embryos were washed with fresh methanol three
632 times before storage at -20°C or future processing.
633
634 For immunohistochemistry, embryos were sequentially rehydrated with increasing percentage of
635 PBSTx (PBS with 0.1% TritonX100) and then washed six times with PBSTx before a one-hour
636 block using 1% BSA in PBSTx at room temperature. Primary antibodies were incubated
637 overnight at 4C and then washed six times in PBSTx. Secondary antibodies in 1% BSA in
638 PBSTx were incubated for two hours at room temperature, washed six times in PBSTx.
639 Embryos were then equilibrated in Vectashield (Vector Laboratories, H-1200) overnight at 4ºC
640 before mounting on coverslips.
641
642 Fluorescent *in situ* hybridization was done as previously shown[78]. Probes were generated using
643 *Drosophila* clones from DGRC (*jhamt* #11840, clone AT13581) and (*Nano*s #1124533, clone
644 RE53469).
645
646
647 mRNA quantification by qPCR
648 RNA was obtained by TRIzol (Invitrogen #15596018) extraction. DNA was removed using RQ1
649 RNase-Free Dnase (Promega #M6101). cDNA was generated using SuperScript III Reverse
650 Transcriptase (Fisher Scientific #18080-044) using both oligo dT and random hexamers.
651 Primers used are listed in Table 3. qPCR was carried out using LightCycler 480 SYBR Green I
652 Master 2X (Roche #04887352001) and a Roche LightCycler 480. Results were calculated as
653 previously described[79] from crossing points and normalized to one of three reference genes
654 found to have invariant expression across tissues and developmental stages: *DCTN2-p50*, *und*,
655 *DCTN5-p25*[80].
656
657
658 Evaluation of JH titers by quantitative mass spectrometry
659 The following genetic backgrounds were used to measure JH III and JHB_3 titers:
660 $jhamt^{8F2/12F1}$ paired with the w^{1118}*; CyO, ft-lacZ* genotype, which was the genetic background the
661 crispr alleles were extensively crossed into and met^{1}, gce^{Mi} paired with w^{1118}. Twenty-five third
662 instar larvae per biological replicate were collected from sparsely populated vials, washed in
663 PBS before placing in 50µl of pre-chilled PBS for hemolymph collection. To collect hemolymph,
664 the cuticle was pinched and pulled apart down the length of the animal. Care was taken not to
665 rupture fat body or intestines. Hemolymph was transferred to pre-chilled silanized glass vials
666 (Fisher Scientific #C4011S5 and #C401154B) using silanized glass pipettes (Brain Bits #FPP).

667 The glass collection well was rinsed with 50µl additional, pre-chilled PBS to obtain any
668 remaining hemolymph and additional PBS was added to silanized glass vials for a total volume
669 of 150µl. Deuterated JH III (62.5pg) dissolved in acetonitrile (Thermo Fisher #51101) was added
670 to each replicate, then 600µl hexane (Sigma Aldrich #1037011000). Samples were vortexed for
671 1 minute and centrifuged for 5 min at 2000g at 4°C. Organic phase was transferred to new
672 silanized vial for analysis by mass spectrometry.
673
674 For mass spectrometry analysis, the JH III and JH III bisepoxide (JHB_3) amounts present in
675 hemolymph were quantified by liquid chromatography coupled to tandem mass spectrometry
676 (HPLC-MS/MS)[24]. The identification and quantification of JH III and JHB_3 in hemolymph
677 samples was based on multiple reaction monitoring (MRM), using the two most abundant
678 fragmentation transitions: for JH III: 267->235 (primary) and 267->147 (secondary), and for
679 JHB_3: 283->233 (primary) and 283->251 (secondary)[24].
680
681
682 Fecundity measurements
683 Fecundity was measured as previously described[81] and reported as the average number of
684 eggs laid in three- and four-day old females at 25ºC. In each biological replicate, 10-12 females
685 were crossed to 5-6 w^{1118} males to mitigate male fertility defects upon *jhamt* or *met, gce* loss.
686
687
688 Knockdown of *jhamt* in Kc167 Cells
689 To effectively knockdown *jhamt* mRNA, genomic DNA obtained from Kc167 cells using Qiagen's
690 Blood and Tissue Kit (#69506) was used as a template. To target *lacZ*, pBluescript SK plasmid
691 used as a template. dsDNA was generated by Choice Taq Mastermix (Denville Scientific
692 #CB4070-8). Gradient PCR was used to obtain optimal dsDNA templates. dsRNAs were
693 generated from dsDNA templates using T7 MEGAScript (Invitrogen #am1334) according to
694 standard protocol. dsRNAs were DNAse treated (Qiagen #79254) and purified using Qiagen
695 RNAeasy Mini Kit (Qiagen #74104) according to instructions. For transfection, Kc167 cells were
696 grown to confluency, resuspended in fresh Schneider's media (Fisher #21720-001)
697 supplemented with Penn/Strep (Fisher, #15140122) and 10% heat inactivated FBS (Thermo
698 Fisher #16140071) to 1x10^6 cells/ml and allowed to settle overnight. 2µg of dsRNAs were
699 used in conjunction with Effectene Transfection Reagent (Qiagen #301425) into each 6-well
700 dish. After 48 hours at 25ºC, media was removed, transfected Kc167 cells were washed in PBS
701 and resuspended in serum-free Schneider's Media (with Penn/Strep) for three additional days at
702 25ºC prior to collection of Kc167-conditioned media. To determine whether *jhamt* knockdown
703 compromised Kc167 viability, the number of Kc167 cells was counted on the day conditioned
704 media was collected. Knockdown efficiency was determined in Kc167 cells by qPCR when
705 conditioned media was collected for the transwell assay. Primers used to measure knockdown
706 efficiency were chosen outside of region targeted by dsRNAs.
707
708
709 Isolation of PGCs

710 *Drosophila* embryos carrying the *P[nos-Moe::eGFP.nos 3'UTR]* transgene from an overnight
711 collection were dechorionated in 50% bleach for two minutes, rinsed and placed in filter-
712 sterilized Chan and Gehring's Balanced Saline, PGC Sort Buffer (3.2g/L NaCl, 3.0g/L KCl,
713 0.69g/L CaCl2.2H2O, 3.7g/L MgSO4.7H2O, 1.79g/L Tricine buffer (pH 7), 3.6g/L glucose,
714 17.1g/L sucrose, 1g/L BSA, fraction V). Dechorionated embryos were manually homogenized in
715 PGC Sort Buffer with Dounce homogenizer (Pyrex #7727-15) and passed through a 100µm filter
716 and 20µm filter and placed in pre-chilled polypropylene falcon tubes (#352063). Live, GFP-
717 positive *Drosophila* PGCs were sorted using a MoFlo XDP cell sorter fitted with a 70µm nozzle
718 into Maxymum recovery microtubes (Axygen #311-05-051) containing 200µl Schneider's Media.
719
720 To enrich for mouse PGCs by FACS, B6; CBA-Tg(Pou5f1-EGFP)2Mnn/J (Jax #004654) mice
721 were bred to produce embryos homozygous for the *Oct*Δ4PE::GFP transgene. Embryonic day
722 0.5 (E0.5) was assumed to be noon of the day the vaginal plug was observed. Pregnant
723 females were euthanized by carbon dioxide followed by cervical dislocation. Trunks were
724 dissected from E10.5 embryos in chilled PBS. For each two embryos, tissue was dissociated in
725 300µl of 0.5% trypsin (0.25%, Life Technologies #25200056) for 15 min at 37ºC, with occasional
726 manual disruption by pipette. Trypsin was inactivated with 200µl of mouse PGC culture media
727 [DMEM/F-12 (Thermo Fisher #11-320-033), 250µM sodium pyruvate (Thermo Fisher
728 #11360070), 2mM L-glutamate (Gibco #25030081), 1X MEM Non-essential amino acids
729 (Thermo Fisher #11-140-050) containing 25% Bovine Albumin Fraction V (Thermo Fisher
730 #15260037). Dissociated tissue was centrifuged at 200g for 7 min and cells were resuspended
731 in 2mL of PGC media. Cell suspension was filtered through a 35µm cell strainer into a 5 ml
732 falcon round bottom tube (VWR #21008-948) for sorting using a MoFlo XDP cell sorter fitted
733 with a 100µm nozzle. Live, GFP+ germ cells were sorted into Maxymum recovery microtubes
734 (Axygen #311-05-051) containing mouse PGC media.
735
736
737 *in vitro* Migration Assays
738 For *in vitro* transwell assays, all plastic ware, tips, tubes and transwell plates used throughout
739 the assay were pre-coated with PBS containing 1% BSA to prevent hydrophobic molecules from
740 sticking to the surfaces. Assays with light sensitive isoprenoids were done in dark conditions as
741 much as possible. For Kc167-conditioned media, serum-free media was added to washed,
742 confluent Kc167 cells and collected three days later. Conditioned media was collected and
743 centrifuged 4,000rpm for 20 min to remove all cellular debris and placed on ice. All isoprenoids
744 (Supplementary Table 4) were prepared by dilution series in either serum-free Schneider's
745 media for *Drosophila* PGC assays or mouse PGC media. Transwell assays were done using the
746 96-well ChemoTx Disposable Chemotaxis System (NeuroProbe #116-10) which had a standard
747 PCTE filter membrane with 10µm pore size, 300µl well capacity and 5.7mm cell site diameter.
748 Sorted germ cells recovered on ice for 30 min while the transwell system was set up. Sorted
749 germ cells were then diluted 10-15-fold in serum-free Schneider's media for *Drosophila* PGC
750 assays or mouse PGC media so that 60µl diluted PGCs were placed above each well.
751 Transwell plates with *Drosophila* PGCs were incubated 25ºC for 1.5 hours and those with
752 mouse PGCs were incubated at 37ºC for 2 hours. After the incubation period, PGCs were
753 removed from above membrane, the plate was centrifuged at 460rpm for 10min to dislodge cells

754 from the well side of the membrane. Translocated germ cells were removed from the 96-well
755 plate by pipetting up and down and transferring to Nunc Lab-Tek II Chambered Coverglass
756 (Thermo Fisher #155409) for manual quantification by fluorescent microscopy.
757
758 The number of PGCs in each top well was calculated by setting aside 10% input (6µl) in
759 duplicate into Lab-Tek wells, each with 300µl serum-free media at the beginning of the transwell
760 assay and quantifying the number of germ cells when the experimental translocated germ cells
761 were quantified. To compare biological replicates done on different days, Specific Migration was
762 calculated by first subtracting the number of germ cells that translocated in the negative control
763 wells (serum-free media) and then calculating the percentage of normalized experimental
764 condition to the respective positive control. Each transwell assay is the result of two to four
765 biological replicates, each consisting of two technical replicates.
766
767
768 Verification of Hormone Activity *in vitro*
769 To verify the activity of JH III and 20-hydroxecdysone (Supplemental Table 4), hormones were
770 added to 50% confluent Schneider 2 (S2) cells at the concentrations indicated in Supp Fig 3c.
771 After a six-hour incubation at 25ºC, S2 cells were harvested, and mRNA was extracted and
772 analyzed using protocols described in the '*mRNA quantification by qPCR*' Methods subsection.
773
774
775 Transcriptional Inhibition in *Drosophila* PGCs
776 Efficient inhibition of transcription in *Drosophila* PGCs isolated by FACS was determined by
777 testing different concentrations of Actinomycin D and Flavopiridol (See Supplemental Table 4).
778 To visualize transcription by immunohistochemistry, Lab-Tek II 8-chambered coverglass were
779 incubated with poly-L-Lysine solution (Sigma-Aldrich #P4707) for 30 min at room temperature
780 and then dried for 1.5 hours. Sorted *Drosophila* PGCs were added to chambers and incubated
781 with Actinomycin D or Flavopiridol for either 15 min or 3 hours, then fixed with 4%
782 paraformaldehyde for 15 minutes, washed in 0.05% PBS with TritonX100, blocked in 1% BSA
783 for 30 min and stained for Vasa, RNA Pol II Ser2CTD and RNA Pol II Ser5 CTD (See
784 Supplemental Table 2 for antibody information). As expected[34], Flavopiridol rapidly inhibited
785 transcription in *Drosophila* PGC while not compromising cell viability. For transwell assays,
786 sorted *Drosophila* PGCs were first incubated with 1µM Flavopiridol for 30 min prior to placing on
787 transwell membrane and solutions in the bottom well chambers also contained 1µM Flavopiridol
788 to ensure PGC transcription was inhibited throughout the assay.
789
790
791 Microscopy and Image Processing
792 Most embryos and other samples were imaged with a Zeiss LSM800, an upright laser scanning
793 confocal microscope using Zen Blue 2.3 software and a Plan-Apochromat 20x 0.8 NA air
794 objective and 40x 1.3NA oil objectives with pinhole size for all imagine was set to 1AU. Images
795 were processed using ImageJ/FIJI.
796
797

798
799 Statistics
800 Statistical analysis was done as described in the Figure Legends. Briefly, for quantification of
801 phenotypic data, such as extragonadal PGC quantification, data was not always normally
802 distributed and thus median +/- IQR are reported, and statistical significance was assessed by
803 Mann-Whitney U test. For mRNA Fold Change and *in vitro* Specific Migration results, mean +/-
804 standard deviation is reported and statistical significance was tested by unpaired t-test. Sample
805 size per biological replicate was influenced by power analysis based on previously observed
806 phenotypic variation.
807
808
809
810
811
812
813
814
815 **Supplemental Table 1:** Animal lines used in this study
816

Name	Species	Source	Notes
P[JHREWt8x-eGFP]attp2	*Drosophila*	This study	JH responsive reporter, with non-specific activity in hemocytes
P[JHREMut8x-eGFP]attp2	*Drosophila*	This study	Negative control reporter transgene with non-specific activity in hemocytes
y^1,w^*, $gce^{mi02742}$	*Drosophila*	BL60189	Insertion that leads to RNA null
Met^1	*Drosophila*	BL3472	EMS-generated from OregonR-C causing G1161736A, DNA mutation and G166D protein change, genetically amorphic allele [82] [31]
y^+, w^+, v^+, Met^1, $gce^{mi02742}$/*Fm7ai*	*Drosophila*	This study	Recombinant between existing mutants listed above
w-, v-, Met^{27}, $gce^{2.5k}$/*Fm7ai*	*Drosophila*	Rebecca Spokony and Lynn Riddiford [83]	Both Met^{27} and $gce^{2.5k}$ are large deletions that lead to full loss of RNA
w^{1118}; $jhamt^{8F2}$ or ^{12F1}/*CyO, ft-lacZ*	*Drosophila*	This study	CRISPR-generated small deletions
$jhamt^{Df(2L)BSC781}$/*CyO, ft-lacZ*	*Drosophila*	BL27353	2L:16325113;16417726, including *jhamt* and 13 other genes
$Hmgcr^{26.31}$/*Tm3, Sb, Ubx-lacZ*	*Drosophila*	[84]	Also known as clb^2
$Hmgcr^{11.54}$/*Tm3, Sb, Ubx-lacZ*	*Drosophila*	[84]	Also known as clb^1
$Hmgcr^{01152}$/*Tm3,Sb, Ubx-lacZ*	*Drosophila*	[19]	L(3)01152 source: Transposon insertion 179 nucleotides into *Hmgcr* locus
UAS-Hmgcr	*Drosophila*	[19]	pNB36C *Hmgcr* cDNA downstream of UASt
y,w; ; UAS-jhamt	*Drosophila*	Ryusuke Niwa [17]	RN286 and RN287, both on the third chromosome, containing two point mutations also found in w^{1118} (F166Y and S182N)
w-; elav-GAL4	*Drosophila*	J Treisman	Second chromosome
w-; 48Y-GAL4	*Drosophila*		Second chromosome
w-; twi-GAL4; 24B-GAL4	*Drosophila*	M. Akam	Second and third chromosome
y,w;; Tub-GAL4	*Drosophila*		Third chromosome
w-, P[nos-moesin::egfp::nos 3'UTR]	*Drosophila*	[85]	
Oct4ΔPE::GFP	Mouse	Jax #004654	B6; CBA-Tg(Pou5f1-EGFP)2Mnn/J

817
818
819

820
821 **Supplemental Table 2:** Antibodies used in this study

Name	Source	Species	Concentration
Vasa	Lehmann lab	Rabbit	1:5,000
GFP	AVES #1020	Chicken	1:500
GFP	Thermo Fisher Scientific #A11122	Rabbit	1:1,000
Singed (fascin)	DSHB #sn 7c	Mouse	1:100
Elav	DSHB #9F8A9	Mouse	1:500
b-galactosidase	Abcam #ab9361	Chicken	1:500
Hindsight	DSHB #1G9	Mouse	1:20
RNA Pol II Ser5	Chromotek #3e8-1	Rat	1:100
RNA Pol II Ser2	Abcam #ab5095	Rabbit	1:500

822
823
824
825
826 **Supplemental Table 3:** Primers used in this study

Element	Purpose	Forward Primer	Reverse Primer
jhamt	Genotyping deletions	AGGTGCAAAGGCACGAT	AGGTGCAAAGGCACGAT
jhamt	Crispr guide	CTTCGAGATCCTGAACCCACATCC	AAACGGATGTGGGTTCAGGATCTC
jhamt	*in situ* probe	GGCACGATGCCAAATTGAT	GATAATACGACTCACTATAGGGGATGTGTAGGCTC CAGGAAA
Nanos	*in situ* probe	AGATTGCGCGATCCTTGAA	TAATACGACTCACTATAGGGCTGGATTCGCCCTCT CTAAAC
und	reference for qPCR	GCAAGAAAAGCGGTCAGACT	CGTGTTGATACGGTCCAGAG
Dnm/DCT N2-p50	reference for qPCR	AGACGCCTGGAAGTAAGCAG	GTAAGGCGGCTCAACTTGTC
DCTN5-p25	reference gene for qPCR	ACAAAGTTAGTCGCCACACG	ATGACGGAGTTCTTGCCAAT
twinstar	Detect DNA contamination	TCAGAGGTGCCTTGACACTG	GATGTGGAGACTGTGGCAGA
eGFP	mRNA quantification	GAACCGCATCGAGCTGAA	TGCTTGTCGGCCATGATATAG
gce	Genotyping and mRNA quant	GGATGCCATCGATCGCAAGT	GCTTCGTCACTACGCCGAAA
Met	Genotyping *met*[1] allele	CTGCTTCCTCACCCTAACCT	CTGCTTCCTCACCCTAACCT
jhamt	mRNA quantification	TGACCATGTCACCTCGTTCTACTGC	GAAGTCATCCAGGAACTGTTCATGC
jhamt	dsRNA 1 for knockdown in Kc167 cells	TAATACGACTCACTATAGGGCCTCACG CCTTCATAAACAA	TAATACGACTCACTATAGGGGGTAACGTGCTCATG GACT
jhamt	dsRNA 2 for knockdown in Kc167 cells	TAATACGACTCACTATAGGGCTTCGTA AAGCCACTGCTCC	TAATACGACTCACTATAGGGCCTCGCCAGGACTTA GACTG
lacZ	dsRNA knockdown DRSC42733	TAATACGACTCACTATAGGG CTGGCGTAATAGCGAAGAGG	TAATACGACTCACTATAGGG CATTAAAGCGAGTGGCAACA
jhamt	Knockdown efficiency	CAGTTCCTGGATGACTTCATAGAC	CCACCACCAATTTATAGGGAGATAG
Kr-h1	JH responsiveness	GAATACGACATAACAGCC	CGATTTCCGTGAATATGTTCT
Eip74b	20E responsiveness	GTACGCGTATTGGGACTATCAG	CACGCGAGATAGGGATTTCTT
Eip75	20E responsiveness	GTCCATCAGCGAGTTGGTATC	CACCAGCAGCCATCTGAA

827
828 **Table 4:** Reagents used in this study
829

Name	Source	Product Number	Stock solvent	Final Concentration
JH III	Sigma-Aldrich	J2000-10MG	Ethanol	0.25-25μM
Methoprene	Sigma-Aldrich	33375-100MG	Ethanol	2.5μM
20-hydroxecdysone	Sigma-Aldrich	H5142-5MG	Ethanol	0.25-25μM
ATRA	Sigma-Aldrich	R2625-50MG	DMSO	2.5μM
9cis-RA	Sigma-Aldrich	R4643	DMSO	2.5μM
Flavopiridol	Selleck	S1230	PBS with 0.1% BSA	1μM
Actinomycin D	Sigma-Aldrich	A1410-Smg	DMSO	1-5μg/mL
CXCL12/Sdf-1a	R&D Systems	460-SD-010	PBS with 0.1% BSA	50ng/mL

830
831
832
833
834
835
836
837
838
839
840
841
842
843
844
845
846
847
848
849
850
851
852
853
854
855

856 **Figure Legends**

857

858 **Figure 1: Juvenile hormone (JH) signaling is active in the embryonic mesoderm during**
859 **PGC migration A** *Left*: Schematic summarizing gonadotropic effect of JH in insects, whereby
860 JH is produced in an endocrine gland and acts systemically to promote oogenesis. *Right*:
861 Summary of established JH signaling pathways wherein endocrine cells produce JHs
862 downstream of Acetyl-CoA and a biosynthetic pathway that culminates in JH acid
863 methyltransferase (Jhamt)-mediated JH production. JHs (red jagged lines) are then secreted in
864 the hemolymph and enter JH-responding cells. Once in JH-responding cells, JH binds to one of
865 two JH transcriptional receptors, Methoprene tolerant (Met) or Germ cell expressed (Gce). JH-
866 bound Met/Gce translocates to the nucleus to regulate target genes. **B** Lateral view images of a
867 late Stage 12 embryo stained by Fluorescent *in situ* hybridization (FISH) for *jhamt* (green) and
868 *nanos* (magenta) mRNA. Primers used to generate *in situ* probes are listed in Supplementary
869 Table 3. *Right:* Magnified image of *jhamt* and *nanos* mRNA in the boxed area outlined by a
870 dashed, white square. **C** Schematic of germ cell development during Stage 10-14 of *Drosophila*
871 embryogenesis. **D** *Top*: schematic of a new transgenic JH sensor (JHRE-GFP) in which eight
872 copies of the JH Response Element from the *early trypsin* gene from *A. aegypti* were placed
873 upstream of eGFP (See Materials and Methods for construct design). *Bottom*: Induction of *Kr-h1*
874 mRNA, a known JH transcriptional target, and *GFP* mRNA. deltaCt was calculated relative to
875 the average Ct of two housekeeping genes, *DCTN5-p25* and *Und*, and fold change was
876 calculated for whole second instar larvae fed cornmeal food containing 1.6μg/mg of JH
877 analogue, methoprene normalized to age and genotype-matched larvae fed ethanol. Animals
878 were fed methoprene or solvent control for 24 hours prior to RNA isolation. Bars and error bars
879 represent average fold change and standard deviation from three biological replicates, each
880 consisting of ten second instar larvae. **E** Dorsal (d) images of Stage 10 *JHRE-GFP* embryos
881 that are wild type (left) or mutant for Met and Gce (right). **F** *Left:* dorsal view of a Stage 11
882 *JHRE-GFP* embryo stained for GFP (green) protein, Vasa (magenta) protein, and DNA using
883 DAPI (gray). *Right*: lateral view of a Stage 11 JHRE-GFP embryo. GFP channel is shown below
884 each merged image. For all images, magnified images in the boxed area outlined by a dashed,
885 white square are shown to the right of each whole-embryo image. Genotypes are noted in the
886 top left corner, embryo orientation in the bottom, and scale bars represent 25μm. All images are
887 maximum projections of two to three 2μm confocal slices.

888

889

890 **Figure 2: Key JH synthesis enzyme, Jhamt, facilitates PGC migration to the gonad.**
891 **A** Schematic of the *jhamt* locus noting the location of premature stop codons within the
892 methyltransferase domain (shown in green), which were introduced by CRISPR-mediated
893 editing. Light gray denotes 5' and 3' UTR. **B** Titers of two JHs, JH III and JH bisepoxide (JHB_3),
894 in hemolymph of third instar *Drosophila* larvae measured by quantitative mass spectrometry
895 using deuterated standards. Each dot represents a biological replicate of hemolymph bled from
896 25 larvae. For titers, w^-*, Sp/CyO,ft-lacZ* was used as a wildtype strain as the CRISPR-induced
897 alleles in a w^- background were initially crossed into this background. **C** Fecundity of young
898 females. Each dot represents the average number of eggs laid per biological replicate, which
899 was obtained by dividing the number of eggs laid over a 24-hour period by the number of
900 females (10-12) in each cohort three- and four-days after eclosion. To avoid confounding male
901 infertility effects, all virgin females were mated to wildtype (w^{1118}) males. For B and C, bars and
902 whiskers represent mean +/- standard deviation and statistical significance was tested by
903 unpaired student t test. **D** Dorsal view images of Stage 14 *Drosophila* embryos stained for Vasa
904 (magenta) and DNA (DAPI, gray). Zygotic genotypes are noted in the top left corner. Gonads
905 are circled with a white dashed circle. Arrowheads highlight extragonadal germ cells. All embryo
906 images are maximum projections of two to three 2µm confocal slices. Scale bars represent
907 25µm. **E** Quantification of extragonadal PGCs in Stage 14-16 embryos. Each dot represents
908 one embryo. To yield $jhamt^{-/-}$ embryos, with heteroallelic combinations of independently derived
909 indels, $jhamt^{8F1}$*/CyO,ftz-lacZ* females were mated to $jhamt^{12F1}$*/CyO,ftz-lacZ*. To generate $jhamt^{-}$
910 $^{/Def}$ embryos, $jhamt^{8F1}$*/CyO,ftz-lacZ* animals were mated to *Df(2L)BSC781/CyO, ft-lacZ* animals.
911 **F** Quantification of extragonadal PGCs in Stage 14-16 embryos when Hmgcr is ectopically
912 expressed in the nervous system using *Elav-GAL4* and *UAS-Hmgcr*. Each dot represents an
913 embryo. For panels E and F, bars and whiskers represent median +/- interquartile range (IQR),
914 statistical significance was tested by Mann-Whitney U test, with ns=not significant. The
915 reference strain for *jhamt* studies was w^{1118} as *jhamt* alleles were backcrossed into this
916 background.
917
918
919
920
921
922
923

924 **Figure 3: Juvenile hormone is sufficient for PGC migration**. **A** Ventral view images of Stage
925 14 embryos stained for Vasa (magenta) and Elav (green). Genotypes are noted in the top left
926 corner of each image. Arrowheads highlight germ cells in contact with Elav-positive central
927 nervous system. All embryo images are maximum projections of two to three 2μm confocal
928 slices. Scale bars represent 25μm. **B** Quantification of the number of PGCs in Stage 14-16
929 embryos contacting Elav-positive cells upon ectopic expression of either *Hmgcr* or *Jhamt* using
930 the *Elav-GAL4* driver. Bar and whiskers represent mean +/- standard deviation and statistical
931 significance was tested by unpaired t-test. **C** *Top Left*: Scatter plots from FACS of GFP-positive
932 PGCs from *nos-moesin::GFP* transgenic embryos. Region 1 (R1) denotes collection cutoff. *Top*
933 *Right*: Image of isolated GFP-positive PGCs (gray). *Bottom*: Schematic of the *in vitro* transwell
934 assay in which FACS-enriched PGCs are placed on a 10μm filter above either serum-free
935 media conditioned with Kc167 cells as a positive control, serum-free unconditioned media as a
936 negative control, or experimental conditions, such as serum-free media with JH III. The number
937 of PGCs that translocated to the bottom well was quantified visually after 1.5 hours. **D**
938 Quantification of Specific PGC migration, which is the percentage of experimental translocated
939 PGCs relative to positive (serum-free Kc167-conditioned media) and negative (serum-free
940 media) controls. Such normalization is required to compare biological replicates done on
941 different days. See Materials and Methods for further details. Numbers shown in white within
942 each *jhamt* knockdown bar represents the Fold Change (FC) of *jhamt* mRNA at the time when
943 conditioned media was collected. Bar height represents mean and error bars represent standard
944 deviation from two to four biological replicates and statistical significance was tested by
945 unpaired t-test. **E** Quantification of specific migration in transwell assays using isolated PGCs
946 placed above serum-free media containing various concentrations of commercially available JH
947 III (green bars) or 20-hydroxyecdysone (20E, magenta bars) with 1% BSA as a non-specific
948 carrier protein. Bars represent means and error bars represent standard deviation from three
949 biological replicates, which were each obtained by averaging two to three technical replicates. **F**
950 Percentage Specific PGC migration wherein isolated PGCs were placed across either serum-
951 free media conditioned (gray), serum-free media with 1% BSA (black) and either JH III (dark
952 green, 2.5μM) or the JH analogue, methoprene, (light green, 2.5μm) with 1% BSA as a non-
953 specific carrier protein. Bars represent means and error bars represent standard deviation from
954 two biological replicates, which were each obtained by averaging two to three technical
955 replicates. ns=not significant.
956
957

958 **Figure 4: JH transcriptional receptor loss compromises PGC migration to the gonad**
959 **A** Schematic of genetic loci encoding the two redundant JH transcriptional receptors, Met and
960 Gce with location of extant mutations recombined for this study noted. **B** Fold change of *gce*
961 and *Kr-h1* mRNAs in *met, gce* mutant one-day old adult females relative to wildtype control
962 animals. deltaCt was calculated relative to the average Ct of *DCTN5-p25* and *Und*. Shown are
963 Fold Change in homoallelic combination for the newly recombined mutant alleles Met^{1}, gce^{Mi}
964 (dark blue) and heteroallelic combination of Met^{1}, gce^{Mi} with existing or Met^{27}, $gce^{2.5k}$ alleles
965 (light blue). Bars and error bars represent mean +/- standard deviation from three biological
966 replicates, each containing pooled mRNA from five females. **C** Fecundity of young females.
967 Each dot represents the average number of eggs laid per biological replicate, which were
968 obtained by dividing the number of eggs laid over a 24-hour period by the number of females
969 (10-12) in each cohort three- and four-days after eclosion. To avoid any confounding male
970 infertility effects, all virgin females were mated to wildtype (w^{1118}) males. Bars and whiskers
971 represent mean +/- standard deviation and statistical significance was tested by unpaired
972 student t test. **D** *Left*: Lateral view images of Stage 14 embryos stained for Vasa (magenta) and
973 DAPI (gray). Maternal and zygotic genotypes are noted in the top left corner. *Right*:
974 Quantification of extragonadal PGCs in Stage 14-16 embryos. Each dot represents one embryo.
975 To generate maternal and zygotic mutant embryos, mutant $Met^{1/27}$, $gce^{Mi/2.5k}$ mothers were
976 crossed to Met^{1},gce^{Mi}/*Y* males. Arrowheads point to extragonadal germ cells. **E** *Top panel*:
977 schematic of genetic suppression experiment. In otherwise wildtype embryos, ectopic
978 expression of *Hmgcr* in the gut/endoderm (green) with *48Y-GAL4; UASt-Hmgcr* transgenes
979 traps ~65% of PGCs (pink) in the gut (*left schematic*). To determine if Met and Gce is required
980 downstream of Hmgcr/JH, $Met^{1/27}$, $gce^{Mi/2.5k}$ females were crossed *48Y-GAL4; UASt-Hmgcr*
981 males to generate PGCs without maternal loading of Met/gce. *Bottom panels*: Lateral view of
982 Stage 14 embryos stained for Vasa (magenta), the endodermal marker, Hnt (green) and DAPI
983 (gray). Bold M: designates the maternal genotype that PGCs primarily rely on when exiting the
984 endoderm. Bold P: designates the paternal genotype. White brackets indicate germ cells that
985 remain in gut. *Right*: Percentage of PGCs remaining in the gut in Stage 14+ embryos upon
986 expression of *UAS-Hmgcr* using the *48Y-GAL4* driver. Each dot represents one embryo. **F**
987 Quantification of Specific *in vitro* migration when isolated PGCs were treated with 1μM
988 flavopiridol to inhibit transcription (Txn) during and 30 minutes prior to and during the same
989 transwell migration assay described in Fig 3c-f. Specific migration was calculated relative to
990 vehicle control treated PGCs subjected to serum-free media (uncond media, black) and serum-
991 free media conditioned with Kc167 (Cond media, gray). The effect of transcriptional inhibition (-)

992 was measured in PGCs subjected to cond media or containing 5μM JH III (green). Bars
993 represent means and error bars represent standard deviation from two biological replicates,
994 which were each obtained by averaging two technical replicates. Bars and whiskers within each
995 graph represent median +/- interquartile range (IQR). Statistical significance was tested by
996 Mann-Whitney U test, with ns=not significant. Dashed white circles outline the gonad and scale
997 bars represent 25μm in all images.
998
999
1000 **Figure 5: Compensatory feedback loop maintains JH homeostasis in *Drosophila*. A** Titers
1001 of two JHs, JH III and JH bisepoxide (JHB_3), in hemolymph of third instar *Drosophila* larvae
1002 measured by quantitative mass spectrometry using deuterated standards. Each dot represents
1003 a biological replicate of hemolymph bled from 25 $Met^{1/1}$, $gce^{Mi/Mi}$ or w^{1118} third instar larvae. **B**
1004 Fold change of *jhamt* and *Kr-h1* mRNA in $Met^{1/27}$, $gce^{Mi/2.5k}$ embryos 12-16 hours post deposition
1005 (hpd) relative to the wildtype strain obtained by crossing w^{1118} to OregonR. deltaCt was
1006 calculated relative to the average Ct of two housekeeping genes, *DCTN5-p25* and *Und*. Bars
1007 and error bars represent the average fold change and standard deviation from three biological
1008 replicates.
1009
1010
1011 **Figure 6: Model of JH function in PGC migration. A** Quantification of specific *in vitro*
1012 migration wherein isolated *Drosophila* PGCs are placed in a transwell migration system across
1013 Kc167-conditioned media (gray), serum-free media (black), JH III (green, 5μM), all trans retinoic
1014 acid (ATRA, dark blue, 5μM) or 9-cis RA (light blue 5μM). **B** Quantification of specific *in vitro*
1015 migration wherein mouse PGCs were FACS-enriched from trunk tissues dissected from E10.5
1016 *Oct4-GFP* embryos and placed across two positive controls: Fetal Bovine Serum (FBS) or
1017 CXCL12 (50 ng/mL) (gray), serum-free media as a negative control (black) or ATRA (dark blue,
1018 1μM) or 9cis-RA (light blue, 1μM). For A and B, bars and error bars represent mean +/-
1019 standard deviation from at least two biological replicates, which were obtained by averaging two
1020 to three technical replicates. **C** Schematic of model for how JHs ensure migrating PGCs (pink)
1021 colonize the somatic gonad (green) in the *Drosophila* embryo.
1022
1023
1024
1025

1026 **Supplemental Data for Figure 1**
1027 **A** Sequence of the JH response element (JHRE) from the *early trypsin* gene of *A. aegypti* that
1028 contains the JH transcription factor, Met/Gce binding motif highlighted in bold[23]. The six base
1029 pair wildtype JHRE sequence is on top and the JHRE in which the Met/Gce-binding motif was
1030 mutated is on the bottom. Eight copies of each sequence were provided by Marek Jindra[15] and
1031 placed upstream of *eGFP*. **B** Ventral view of Stage 14 embryos carrying a mutated JH
1032 biosensor (*JHRE Mut8x-GFP*) in which the JHRE has been mutated. Embryos were stained for
1033 GFP (green) and the hemocyte marker, Fascin (gray). Right panel is the same image but with
1034 the Fascin signal alone in grayscale. **C** Lateral view of embryos stained for Vasa (magenta),
1035 GFP (green) and DAPI (gray). Genotype is noted above each early Stage 12 and Stage 14 pair.
1036 To the right of each whole-embryo image is the area within the white, dashed box magnified.
1037 Scale bars represent 25μm in all images.
1038
1039
1040 **Supplemental Data for Figure 2**
1041 Nature of the small deletions in *jhamt* created by CRISPR-mediated cutting. Seven founders
1042 generated fifteen lines which possessed small insertions or deletions at the cut site that created
1043 premature stop codons at the beginning of methyl transferase domain of *jhamt* (amino acids 40-
1044 137). Class 1 lines (12F1, 12F2) cause a premature stop codon at amino acid 46, while Class II
1045 mutations (1F1, 1F2, 4F1, 4F3, 6F2, 6F3, 7F2, 7F3, 8F1, 8F2, 12F3, 14M2, 14M3) cause a
1046 premature stop codon at amino acid 54.
1047
1048
1049 **Supplemental Data for Figure 3**
1050 **A** *Left:* Quantification of the number of PGCs in Stage 14-16 embryos that remained in the gut
1051 upon ectopic expression of either *Hmgcr* or *jhamt* using the *48Y-GAL4* driver. *Right:*
1052 Quantification of the number of germ cells in Stage 14-16 embryos that contact Zfh-1-positive
1053 cells upon the expression of either *Hmgcr* or *jhamt* using the *twist(twi)-GAL4* and *24B-GAL4*
1054 drivers. Each dot represents one embryo. Bars and whiskers represent median +/- IQR and
1055 statistical significance was analyzed by the Mann-Whitney U test. **B** Quantification of percent
1056 Kc167 cells, used to condition serum-free media, upon *jhamt* mRNA knocked down relative to
1057 transfection control. Bars and error bars represent mean +/- standard deviation from two
1058 biological replicates, each including at least two technical replicates. **C** Quantification of the fold
1059 change in mRNAs in S2 cells upon incubation with varying concentrations of 20-Ecdysone (20-

1060 E) or JH III for six hours prior to mRNA isolation. mRNAs from two verified ecdysone-responsive
1061 genes were measured: *Eip74b* (lighter purple) and *Eip75* (darker purple) and one JH-responsive
1062 gene was measured, *Kr-h1* (green) and normalized to the housekeeping gene, *DCTN2-p50*.
1063 Error bars represent standard deviation from two biological replicates, each consisting of at
1064 least two technical replicates.
1065
1066
1067 **Supplemental Data for Figure 4**
1068 Confocal images of *Drosophila* PGCs enriched by FACS and stained for Vasa (magenta), RNA
1069 Pol II, Ser5p (green), RNA Pol II, Ser2p (yellow) and DAPI (gray). Bottom panel shows a germ
1070 cell treated with 1μM Flavopiridol for 3 hours. Scale bars represent 5μm.
1071
1072
1073 **Supplemental Data for Figure 5**
1074 **A** Fold change of *jhamt* mRNAs in *Met, gce* mutant one-day old adult females relative to
1075 wildtype control animals. deltaCt was calculated relative to the average Ct of *DCTN5-p25* and
1076 *Und*. Shown are Fold Change of *jhamt* mRNA in adults homozygous for the newly recombined
1077 mutant alleles Met^{1}, gce^{Mi} (dark blue) and heteroallelic combination of Met^{1}, gce^{Mi} with existing
1078 or Met^{27}, $gce^{2.5k}$ alleles (light blue). Bars and error bars represent mean +/- standard deviation
1079 from three biological replicates, each containing pooled mRNA from five females. **B** Schematic
1080 of the Ecdysone Receptor (EcR), Taiman (Tai) and Met binding sites near the *jhamt* locus.
1081 Binding sites were obtained from ModEncode[63].
1082
1083
1084 **Supplemental Data for Figure 6**
1085 **A** Scatter plots from FACS of GFP-positive PGCs enriched from trunks of E10.5 mouse
1086 embryos carrying the *Oct4ΔPE:GFP* transgene. The number inside the gate lines denotes the
1087 percentage of collected events in a typical biological replicate. **B** Quantification of the percent
1088 change in the number of mouse germ cells before and two hours after application of 1μm ATRA
1089 or 9cis-RA. Two hours was chosen because this is the duration of the *in vitro* migration assay.
1090 Graphed is the mean and standard deviation from three biological replicated. Each dot
1091 represents the averaged technical replicates of each biological replicate.
1092
1093

1094 **References**
1095

1096 1. Saitou, M., and Hayashi, K. (2021). Mammalian in vitro gametogenesis. Science *374*,
1097 eaaz6830. 10.1126/science.aaz6830.
1098 2. Finger, D.S., Whitehead, K.M., Phipps, D.N., and Ables, E.T. (2021). Nuclear receptors
1099 linking physiology and germline stem cells in Drosophila. Vitam Horm *116*, 327-362.
1100 10.1016/bs.vh.2020.12.008.
1101 3. Banisch, T.U., Slaidina, M., Gupta, S., Ho, M.G., Gilboa, L., and Lehmann, R. (2021). A
1102 transitory signaling center controls timing of primordial germ cell differentiation. Dev
1103 Cell *56*, 1742-+. 10.1016/j.devcel.2021.05.008.
1104 4. Bai, J.W., Uehara, Y., and Montell, D.J. (2000). Regulation of invasive cell behavior by
1105 taiman, a Drosophila protein related to AlB1, a steroid receptor coactivator amplified in
1106 breast cancer. Cell *103*, 1047-1058. Doi 10.1016/S0092-8674(00)00208-7.
1107 5. Hodin, J., and Riddiford, L.M. (1998). The ecdysone receptor and ultraspiracle regulate
1108 the timing and progression of ovarian morphogenesis during Drosophila
1109 metamorphosis. Dev Genes Evol *208*, 304-317. DOI 10.1007/s004270050186.
1110 6. Olmstead, A.W., and Leblanc, G.A. (2002). Juvenoid hormone methyl farnesoate is a sex
1111 determinant in the crustacean Daphnia magna. J Exp Zool *293*, 736-739.
1112 10.1002/jez.10162.
1113 7. Roy, S., Saha, T.T., Zou, Z., and Raikhel, A.S. (2018). Regulatory Pathways Controlling
1114 Female Insect Reproduction. Annu Rev Entomol *63*, 489-511. 10.1146/annurev-ento-
1115 020117-043258.
1116 8. Santos, C.G., Humann, F.C., and Hartfelder, K. (2019). Juvenile hormone signaling in
1117 insect oogenesis. Curr Opin Insect Sci *31*, 43-48. 10.1016/j.cois.2018.07.010.
1118 9. Luo, W., Veeran, S., Wang, J., Li, S., Li, K., and Liu, S.N. (2020). Dual roles of juvenile
1119 hormone signaling during early oogenesis in Drosophila. Insect Sci *27*, 665-674.
1120 10.1111/1744-7917.12698.
1121 10. Easwaran, S., Van Ligten, M., Kui, M., and Montell, D.J. (2022). Enhanced germline stem
1122 cell longevity in Drosophila diapause. Nat Commun *13*. ARTN 711
1123 10.1038/s41467-022-28347-z.
1124 11. Hiruma, K., and Kaneko, Y. (2013). Hormonal Regulation of Insect Metamorphosis with
1125 Special Reference to Juvenile Hormone Biosynthesis. Curr Top Dev Biol *103*, 73-100.
1126 10.1016/B978-0-12-385979-2.00003-4.
1127 12. Riddiford, L.M. (2020). Rhodnius, Golden Oil, and Met: A History of Juvenile Hormone
1128 Research. Front Cell Dev Biol *8*, 679. 10.3389/fcell.2020.00679.
1129 13. Jindra, M., Tumova, S., Milacek, M., and Bittova, L. (2021). A decade with the juvenile
1130 hormone receptor. Adv Insect Physiol *60*, 37-85. 10.1016/bs.aiip.2021.03.001.
1131 14. Abdou, M.A., He, Q.Y., Wen, D., Zyaan, O., Wang, J., Xu, J.J., Baumann, A.A., Joseph, J.,
1132 Wilson, T.G., Li, S., and Wang, J. (2011). Drosophila Met and Gce are partially redundant
1133 in transducing juvenile hormone action. Insect Biochem Molec *41*, 938-945.
1134 10.1016/j.ibmb.2011.09.003.
1135 15. Jindra, M., Uhlirova, M., Charles, J.P., Smykal, V., and Hill, R.J. (2015). Genetic Evidence
1136 for Function of the bHLH-PAS Protein Gce/Met As a Juvenile Hormone Receptor. Plos
1137 Genetics *11*. ARTN e1005394

1138 10.1371/journal.pgen.1005394.
1139 16. Jindra, M., Belles, X., and Shinoda, T. (2015). Molecular basis of juvenile hormone
1140 signaling. Curr Opin Insect Sci *11*, 39-46. 10.1016/j.cois.2015.08.004.
1141 17. Niwa, R., Niimi, T., Honda, N., Yoshiyama, M., Itoyama, K., Kataoka, H., and Shinoda, T.
1142 (2008). Juvenile hormone acid O-methyltransferase in Drosophila melanogaster. Insect
1143 Biochem Molec *38*, 714-720. 10.1016/j.ibmb.2008.04.003.
1144 18. Oosterhuis, J.W., and Looijenga, L.H.J. (2019). Human germ cell tumours from a
1145 developmental perspective. Nat Rev Cancer *19*, 522-537. 10.1038/s41568-019-0178-9.
1146 19. Van Doren, M., Broihier, H.T., Moore, L.A., and Lehmann, R. (1998). HMG-CoA reductase
1147 guides migrating primordial germ cells. Nature *396*, 466-469. 10.1038/24871.
1148 20. Koubova, J., Menke, D.B., Zhou, Q., Capel, B., Griswold, M.D., and Page, D.C. (2006).
1149 Retinoic acid regulates sex-specific timing of meiotic initiation in mice. P Natl Acad Sci
1150 USA *103*, 2474-2479. 10.1073/pnas.0510813103.
1151 21. Bowles, J., Knight, D., Smith, C., Wilhelm, D., Richman, J., Mamiya, S., Yashiro, K.,
1152 Chawengsaksophak, K., Wilson, M.J., Rossant, J., et al. (2006). Retinoid signaling
1153 determines germ cell fate in mice. Science *312*, 596-600. 10.1126/science.1125691.
1154 22. Bowles, J., Feng, C.W., Miles, K., Ineson, J., Spiller, C., and Koopman, P. (2016). ALDH1A1
1155 provides a source of meiosis-inducing retinoic acid in mouse fetal ovaries. Nature
1156 Communications *7*. ARTN 10845
1157 10.1038/ncomms10845.
1158 23. Noriega, F.G., Shah, D.K., and Wells, M.A. (1997). Juvenile hormone controls early
1159 trypsin gene transcription in the midgut of Aedes aegypti. Insect Mol Biol *6*, 63-66. DOI
1160 10.1046/j.1365-2583.1997.00154.x.
1161 24. Ramirez, C.E., Nouzova, M., Michalkova, V., Fernandez-Lima, F., and Noriega, F.G.
1162 (2020). Common structural features facilitate the simultaneous identification and
1163 quantification of the five most common juvenile hormones by liquid chromatography-
1164 tandem mass spectrometry. Insect Biochem Mol Biol *116*, 103287.
1165 10.1016/j.ibmb.2019.103287.
1166 25. Wen, D., Rivera-Perez, C., Abdou, M., Jia, Q.Q., He, Q.Y., Liu, X., Zyaan, O., Xu, J.J.,
1167 Bendena, W.G., Tobe, S.S., et al. (2015). Methyl Farnesoate Plays a Dual Role in
1168 Regulating Drosophila Metamorphosis. Plos Genetics *11*. ARTN e1005038
1169 10.1371/journal.pgen.1005038.
1170 26. Burtenshaw, S.M., Su, P.P., Zhang, J.R., Tobe, S.S., Dayton, L., and Bendena, W.G. (2008).
1171 A putative farnesoic acid O-methyltransferase (FAMeT) orthologue in Drosophila
1172 melanogaster (CG10527): Relationship to juvenile hormone biosynthesis? Peptides *29*,
1173 242-251. 10.1016/j.peptides.2007.10.030.
1174 27. Zhang, H.Y., Tian, L., Tobe, S., Xiong, Y., Wang, S.Y., Lin, X.D., Liu, Y.A., Bendena, W., Li,
1175 S., and Zhang, Y.Q. (2010). Drosophila CG10527 mutants are resistant to juvenile
1176 hormone and its analog methoprene. Biochem Bioph Res Co *401*, 182-187.
1177 10.1016/j.bbrc.2010.09.019.
1178 28. Kenwrick, K., Mukherjee, A., and Renault, A.D. (2019). Hmgcr promotes a long-range
1179 signal to attract Drosophila germ cells independently of Hedgehog. J Cell Sci *132*.
1180 10.1242/jcs.232637.

1181 29. Santos, A.C., and Lehmann, R. (2004). Isoprenoids control germ cell migration
1182 downstream of HMGCoA reductase. Developmental cell *6*, 283-293.
1183 30. Ricardo, S., and Lehmann, R. (2009). An ABC transporter controls export of a Drosophila
1184 germ cell attractant. Science *323*, 943-946. 10.1126/science.1166239.
1185 31. Wilson, T.G., Wang, S., Beno, M., and Farkas, R. (2006). Wide mutational spectrum of a
1186 gene involved in hormone action and insecticide resistance in Drosophila melanogaster.
1187 Mol Genet Genomics *276*, 294-303. 10.1007/s00438-006-0138-4.
1188 32. Luo, W., Liu, S.N., Zhang, W.Q., Yang, L., Huang, J.H., Zhou, S.T., Feng, Q.L., Palli, S.R.,
1189 Wang, J., Roth, S., and Li, S. (2021). Juvenile hormone signaling promotes ovulation and
1190 maintains egg shape by inducing expression of extracellular matrix genes. P Natl Acad
1191 Sci USA *118*. ARTN e2104461118
1192 10.1073/pnas.2104461118.
1193 33. Siddiqui, N.U., Li, X., Luo, H., Karaiskakis, A., Hou, H.Y., Kislinger, T., Westwood, J.T.,
1194 Morris, Q., and Lipshitz, H.D. (2012). Genome-wide analysis of the maternal-to-zygotic
1195 transition in Drosophila primordial germ cells. Genome Biol *13*. ARTN R11
1196 10.1186/gb-2012-13-2-r11.
1197 34. Bensaude, O. (2011). Inhibiting eukaryotic transcription: Which compound to choose?
1198 How to evaluate its activity? Transcription *2*, 103-108. 10.4161/trns.2.3.16172.
1199 35. Clagett-Dame, M., and Knutson, D. (2011). Vitamin A in reproduction and development.
1200 Nutrients *3*, 385-428. 10.3390/nu3040385.
1201 36. Busada, J.T., Chappell, V.A., Niedenberger, B.A., Kaye, E.P., Keiper, B.D., Hogarth, C.A.,
1202 and Geyer, C.B. (2015). Retinoic acid regulates Kit translation during spermatogonial
1203 differentiation in the mouse. Dev Biol *397*, 140-149. 10.1016/j.ydbio.2014.10.020.
1204 37. Ghyselinck, N.B., and Duester, G. (2019). Retinoic acid signaling pathways. Development
1205 *146*. 10.1242/dev.167502.
1206 38. Harmon, M.A., Boehm, M.F., Heyman, R.A., and Mangelsdorf, D.J. (1995). Activation of
1207 mammalian retinoid X receptors by the insect growth regulator methoprene.
1208 Proceedings of the National Academy of Sciences of the United States of America *92*,
1209 6157-6160.
1210 39. Knaut, H., Werz, C., Geisler, R., Nusslein-Volhard, C., and Tubingen Screen, C. (2003). A
1211 zebrafish homologue of the chemokine receptor Cxcr4 is a germ-cell guidance receptor.
1212 Nature *421*, 279-282. 10.1038/nature01338.
1213 40. Doitsidou, M., Reichman-Fried, M., Stebler, J., Koprunner, M., Dorries, J., Meyer, D.,
1214 Esguerra, C.V., Leung, T., and Raz, E. (2002). Guidance of primordial germ cell migration
1215 by the chemokine SDF-1. Cell *111*, 647-659. 10.1016/s0092-8674(02)01135-2.
1216 41. Molyneaux, K.A., Zinszner, H., Kunwar, P.S., Schaible, K., Stebler, J., Sunshine, M.J.,
1217 O'Brien, W., Raz, E., Littman, D., Wylie, C., and Lehmann, R. (2003). The chemokine
1218 SDF1/CXCL12 and its receptor CXCR4 regulate mouse germ cell migration and survival.
1219 Development *130*, 4279-4286.
1220 42. Koshimizu, U., Watanabe, M., and Nakatsuji, N. (1995). Retinoic acid is a potent growth
1221 activator of mouse primordial germ cells in vitro. Developmental biology *168*, 683-685.
1222 10.1006/dbio.1995.1113.
1223 43. Campos-Ortega, J.A., and Hartenstein, V. (1997). The embryonic development of
1224 Drosophila melanogaster, 2nd Edition (Springer).

1225 44. De Velasco, B., Shen, J., Go, S., and Hartenstein, V. (2004). Embryonic development of
1226 the Drosophila corpus cardiacum, a neuroendocrine gland with similarity to the
1227 vertebrate pituitary, is controlled by sine oculis and glass. Dev Biol *274*, 280-294.
1228 10.1016/j.ydbio.2004.07.015.
1229 45. Pecasse, F., Beck, Y., Ruiz, C., and Richards, G. (2000). Kruppel-homolog, a stage-specific
1230 modulator of the prepupal ecdysone response, is essential for Drosophila
1231 metamorphosis. Dev Biol *221*, 53-67. 10.1006/dbio.2000.9687.
1232 46. Graveley, B.R., Brooks, A.N., Carlson, J.W., Duff, M.O., Landolin, J.M., Yang, L., Artieri,
1233 C.G., van Baren, M.J., Boley, N., Booth, B.W., et al. (2011). The developmental
1234 transcriptome of Drosophila melanogaster. Nature *471*, 473-479. 10.1038/nature09715.
1235 47. Rahman, M.M., Franch-Marro, X., Maestro, J.L., Martin, D., and Casali, A. (2017). Local
1236 Juvenile Hormone activity regulates gut homeostasis and tumor growth in adult
1237 Drosophila. Sci Rep-Uk *7*. ARTN 11677
1238 10.1038/s41598-017-11199-9.
1239 48. Bittova, L., Jedlicka, P., Dracinsky, M., Kirubakaran, P., Vondrasek, J., Hanus, R., and
1240 Jindra, M. (2019). Exquisite ligand stereoselectivity of a Drosophila juvenile hormone
1241 receptor contrasts with its broad agonist repertoire. Journal of Biological Chemistry *294*,
1242 410-423. 10.1074/jbc.RA118.005992.
1243 49. Rahman, M.M., Franch-Marro, X., Maestro, J.L., Martin, D., and Casali, A. (2017). Local
1244 Juvenile Hormone activity regulates gut homeostasis and tumor growth in adult
1245 Drosophila. Sci Rep *7*, 11677. 10.1038/s41598-017-11199-9.
1246 50. Baumann, A., Barry, J., Wang, S., Fujiwara, Y., and Wilson, T.G. (2010). Paralogous genes
1247 involved in juvenile hormone action in Drosophila melanogaster. Genetics *185*, 1327-
1248 1336. 10.1534/genetics.110.116962.
1249 51. Tomancak, P., Beaton, A., Weiszmann, R., Kwan, E., Shu, S., Lewis, S.E., Richards, S.,
1250 Ashburner, M., Hartenstein, V., Celniker, S.E., and Rubin, G.M. (2002). Systematic
1251 determination of patterns of gene expression during Drosophila embryogenesis.
1252 Genome Biol *3*, RESEARCH0088. 10.1186/gb-2002-3-12-research0088.
1253 52. Tomancak, P., Berman, B.P., Beaton, A., Weiszmann, R., Kwan, E., Hartenstein, V.,
1254 Celniker, S.E., and Rubin, G.M. (2007). Global analysis of patterns of gene expression
1255 during Drosophila embryogenesis. Genome Biol *8*, R145. 10.1186/gb-2007-8-7-r145.
1256 53. Hammonds, A.S., Bristow, C.A., Fisher, W.W., Weiszmann, R., Wu, S., Hartenstein, V.,
1257 Kellis, M., Yu, B., Frise, E., and Celniker, S.E. (2013). Spatial expression of transcription
1258 factors in Drosophila embryonic organ development. Genome Biol *14*, R140.
1259 10.1186/gb-2013-14-12-r140.
1260 54. Zhang, T.L., Song, W., Li, Z., Qian, W.L., Wei, L., Yang, Y., Wang, W.N., Zhou, X., Meng,
1261 M., Peng, J., et al. (2018). Kruppel homolog 1 represses insect ecdysone biosynthesis by
1262 directly inhibiting the transcription of steroidogenic enzymes. P Natl Acad Sci USA *115*,
1263 3960-3965. 10.1073/pnas.1800435115.
1264 55. Hua, S.J., Kittler, R., and White, K.P. (2009). Genomic Antagonism between Retinoic Acid
1265 and Estrogen Signaling in Breast Cancer. Cell *137*, 1259-1271.
1266 10.1016/j.cell.2009.04.043.

1267 56. Ilenchuk, T.T., and Davey, K.G. (1987). The Development of Responsiveness to Juvenile-
1268 Hormone in the Follicle Cells of Rhodnius-Prolixus. Insect Biochem *17*, 525-529. Doi
1269 10.1016/0020-1790(87)90050-3.
1270 57. Yamamoto, K., Chadarevian, A., and Pellegrini, M. (1988). Juvenile-Hormone Action
1271 Mediated in Male Accessory-Glands of Drosophila by Calcium and Kinase-C. Science *239*,
1272 916-919. DOI 10.1126/science.3124270.
1273 58. Sevala, V.L., and Davey, K.G. (1989). Action of Juvenile-Hormone on the Follicle Cells of
1274 Rhodnius-Prolixus - Evidence for a Novel Regulatory Mechanism Involving Protein
1275 Kinase-C. Experientia *45*, 355-356. Doi 10.1007/Bf01957476.
1276 59. Pszczolkowski, M.A., Peterson, A., Srinivasan, A., and Ramaswamy, S.B. (2005).
1277 Pharmacological analysis of ovarial patency in Heliothis virescens. J Insect Physiol *51*,
1278 445-453. 10.1016/j.jinsphys.2005.01.008.
1279 60. Liu, P., Peng, H.J., and Zhu, J. (2015). Juvenile hormone-activated phospholipase C
1280 pathway enhances transcriptional activation by the methoprene-tolerant protein.
1281 Proceedings of the National Academy of Sciences of the United States of America *112*,
1282 E1871-1879. 10.1073/pnas.1423204112.
1283 61. Zheng, H., Wang, N., Yun, J., Xu, H., Yang, J., and Zhou, S. (2022). Juvenile hormone
1284 promotes paracellular transport of yolk proteins via remodeling zonula adherens at
1285 tricellular junctions in the follicular epithelium. PLoS Genet *18*, e1010292.
1286 10.1371/journal.pgen.1010292.
1287 62. Paquet, M., Parenteau, C., Ford, L.E., Ratz, T., Richardson, J., Angelier, F., and Smiseth,
1288 P.T. (2020). Females adjust maternal hormone concentration in eggs according to male
1289 condition in a burying beetle. Horm Behav *121*. ARTN 104708
1290 10.1016/j.yhbeh.2020.104708.
1291 63. Hammal, F., de Langen, P., Bergon, A., Lopez, F., and Ballester, B. (2022). ReMap 2022: a
1292 database of Human, Mouse, Drosophila and Arabidopsis regulatory regions from an
1293 integrative analysis of DNA-binding sequencing experiments. Nucleic Acids Res *50*,
1294 D316-D325. 10.1093/nar/gkab996.
1295 64. Liu, S., Li, K., Gao, Y., Liu, X., Chen, W., Ge, W., Feng, Q., Palli, S.R., and Li, S. (2018).
1296 Antagonistic actions of juvenile hormone and 20-hydroxyecdysone within the ring gland
1297 determine developmental transitions in Drosophila. Proc Natl Acad Sci U S A *115*, 139-
1298 144. 10.1073/pnas.1716897115.
1299 65. Zhang, T., Song, W., Li, Z., Qian, W., Wei, L., Yang, Y., Wang, W., Zhou, X., Meng, M.,
1300 Peng, J., et al. (2018). Kruppel homolog 1 represses insect ecdysone biosynthesis by
1301 directly inhibiting the transcription of steroidogenic enzymes. Proc Natl Acad Sci U S A
1302 *115*, 3960-3965. 10.1073/pnas.1800435115.
1303 66. Casper, A.L., and Van Doren, M. (2009). The establishment of sexual identity in the
1304 Drosophila germline. Development *136*, 3821-3830. 10.1242/dev.042374.
1305 67. Iwata, M., Hirakiyama, A., Eshima, Y., Kagechika, H., Kato, C., and Song, S.Y. (2004).
1306 Retinoic acid imprints gut-homing specificity on T cells. Immunity *21*, 527-538.
1307 10.1016/j.immuni.2004.08.011.
1308 68. Kim, M.H., Taparowsky, E.J., and Kim, C.H. (2015). Retinoic Acid Differentially Regulates
1309 the Migration of Innate Lymphoid Cell Subsets to the Gut. Immunity *43*, 107-119.
1310 10.1016/j.immuni.2015.06.009.

1311 69. Al Tanoury, Z., Piskunov, A., and Rochette-Egly, C. (2013). Vitamin A and retinoid
1312 signaling: genomic and nongenomic effects. J Lipid Res *54*, 1761-1775.
1313 10.1194/jlr.R030833.
1314 70. Rand, C.D., Spencer, G.E., and Carlone, R.L. (2017). Retinoic acid as a chemoattractant
1315 for cultured embryonic spinal cord neurons of the African Clawed Frog, Xenopus laevis.
1316 Can J Zool *95*, 653-661. 10.1139/cjz-2016-0279.
1317 71. Farrar, N.R., Dmetrichuk, J.M., Carlone, R.L., and Spencer, G.E. (2009). A Novel,
1318 Nongenomic Mechanism Underlies Retinoic Acid-Induced Growth Cone Turning. J
1319 Neurosci *29*, 14136-14142. 10.1523/Jneurosci.2921-09.2009.
1320 72. Vesprini, N.D., Dawson, T.F., Yuan, Y., Bruce, D., and Spencer, G.E. (2015). Retinoic acid
1321 affects calcium signaling in adult molluscan neurons. J Neurophysiol *113*, 172-181.
1322 10.1152/jn.00458.2014.
1323 73. Johnson, A., Nasser, T.I.N., and Spencer, G.E. (2019). Inhibition of Rho GTPases in
1324 Invertebrate Growth Cones Induces a Switch in Responsiveness to Retinoic Acid.
1325 Biomolecules *9*. ARTN 460
1326 10.3390/biom9090460.
1327 74. de Hoog, E., Lukewich, M.K., and Spencer, G.E. (2019). Retinoid receptor-based signaling
1328 plays a role in voltage-dependent inhibition of invertebrate voltage-gated Ca2+
1329 channels. J Biol Chem *294*, 10076-10093. 10.1074/jbc.RA118.006444.
1330 75. Gramates, L.S., Agapite, J., Attrill, H., Calvi, B.R., Crosby, M.A., dos Santos, G., Goodman,
1331 J.L., Goutte-Gattat, D., Jenkins, V.K., Kaufman, T., et al. (2022). FlyBase: a guided tour of
1332 highlighted features. Genetics *220*. ARTN iyac035
1333 10.1093/genetics/iyac035.
1334 76. Yoshimizu, T., Sugiyama, N., De Felice, M., Yeom, Y.I., Ohbo, K., Masuko, K., Obinata, M.,
1335 Abe, K., Scholer, H.R., and Matsui, Y. (1999). Germline-specific expression of the Oct-
1336 4/green fluorescent protein (GFP) transgene in mice. Dev Growth Differ *41*, 675-684.
1337 10.1046/j.1440-169x.1999.00474.x.
1338 77. Restifo, L.L., and Wilson, T.G. (1998). A juvenile hormone agonist reveals distinct
1339 developmental pathways mediated by ecdysone-inducible broad complex transcription
1340 factors. Dev Genet *22*, 141-159. 10.1002/(SICI)1520-6408(1998)22:2<141::AID-
1341 DVG4>3.0.CO;2-6.
1342 78. Lecuyer, E., Necakov, A.S., Caceres, L., and Krause, H.M. (2008). High-resolution
1343 fluorescent in situ hybridization of Drosophila embryos and tissues. CSH Protoc *2008*,
1344 pdb prot5019. 10.1101/pdb.prot5019.
1345 79. Livak, K.J., and Schmittgen, T.D. (2001). Analysis of relative gene expression data using
1346 real-time quantitative PCR and the 2(-Delta Delta C(T)) Method. Methods *25*, 402-408.
1347 10.1006/meth.2001.1262.
1348 80. Celniker, S.E., Dillon, L.A., Gerstein, M.B., Gunsalus, K.C., Henikoff, S., Karpen, G.H.,
1349 Kellis, M., Lai, E.C., Lieb, J.D., MacAlpine, D.M., et al. (2009). Unlocking the secrets of the
1350 genome. Nature *459*, 927-930. 10.1038/459927a.
1351 81. Barton, L.J., Duan, T., Ke, W., Luttinger, A., Lovander, K.E., Soshnev, A.A., and Geyer, P.K.
1352 (2018). Nuclear lamina dysfunction triggers a germline stem cell checkpoint. Nat
1353 Commun *9*, 3960. 10.1038/s41467-018-06277-z.

1354 82. Wilson, T.G., and Fabian, J. (1986). A Drosophila melanogaster mutant resistant to a
1355 chemical analog of juvenile hormone. Developmental biology *118*, 190-201.
1356 10.1016/0012-1606(86)90087-4.
1357 83. Baumann, A.A., Texada, M.J., Chen, H.M., Etheredge, J.N., Miller, D.L., Picard, S.,
1358 Warner, R., Truman, J.W., and Riddiford, L.M. (2017). Genetic tools to study juvenile
1359 hormone action in Drosophila. Sci Rep *7*, 2132. 10.1038/s41598-017-02264-4.
1360 84. Moore, L.A., Broihier, H.T., Van Doren, M., Lunsford, L.B., and Lehmann, R. (1998).
1361 Identification of genes controlling germ cell migration and embryonic gonad formation
1362 in Drosophila. Development *125*, 667-678.
1363 85. Sano, H., Renault, A.D., and Lehmann, R. (2005). Control of lateral migration and germ
1364 cell elimination by the Drosophila melanogaster lipid phosphate phosphatases Wunen
1365 and Wunen 2. The Journal of cell biology *171*, 675-683. 10.1083/jcb.200506038.
1366

Figure 1
JH signaling is active in the embryonic mesoderm during PGC migration

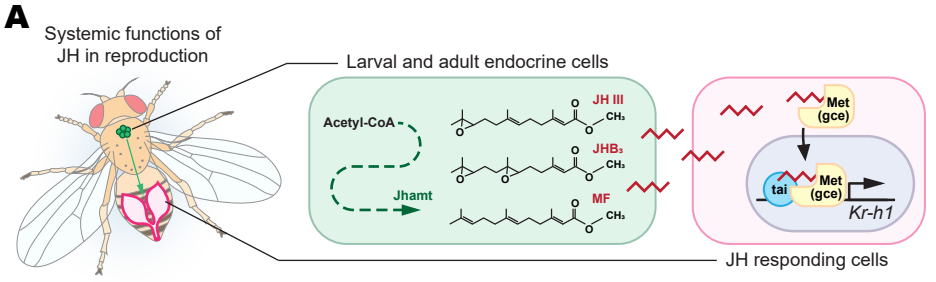

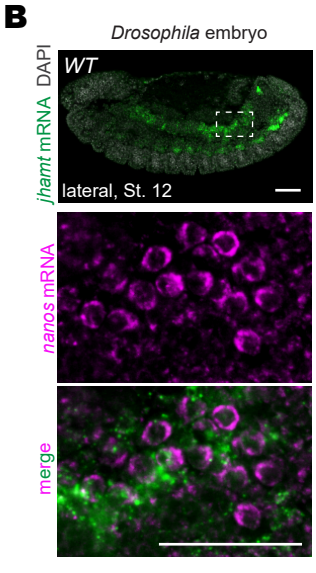

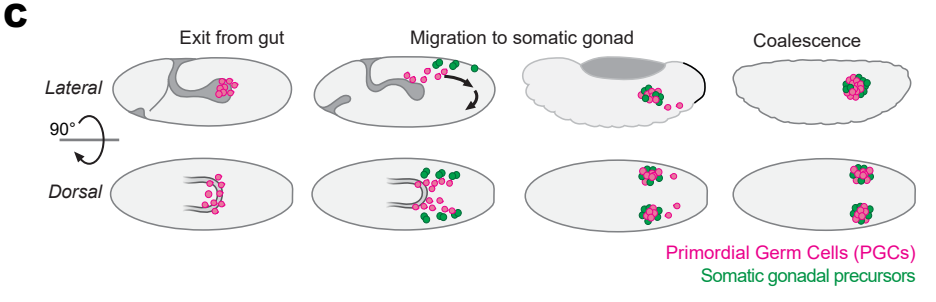

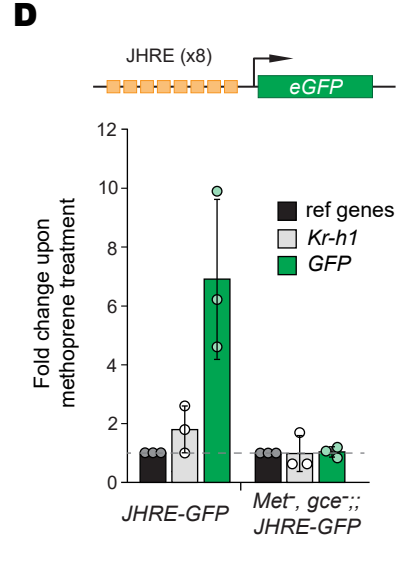

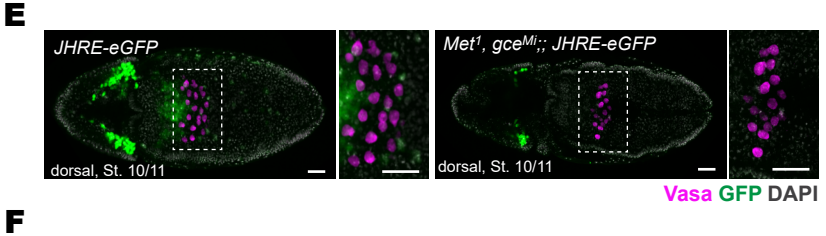

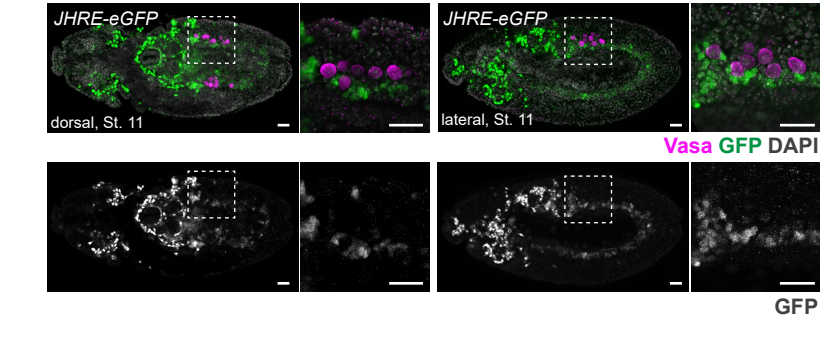

Figure 2
Key JH biosynthesis enzyme, Jhamt, facilitates PGC migration to the gonad

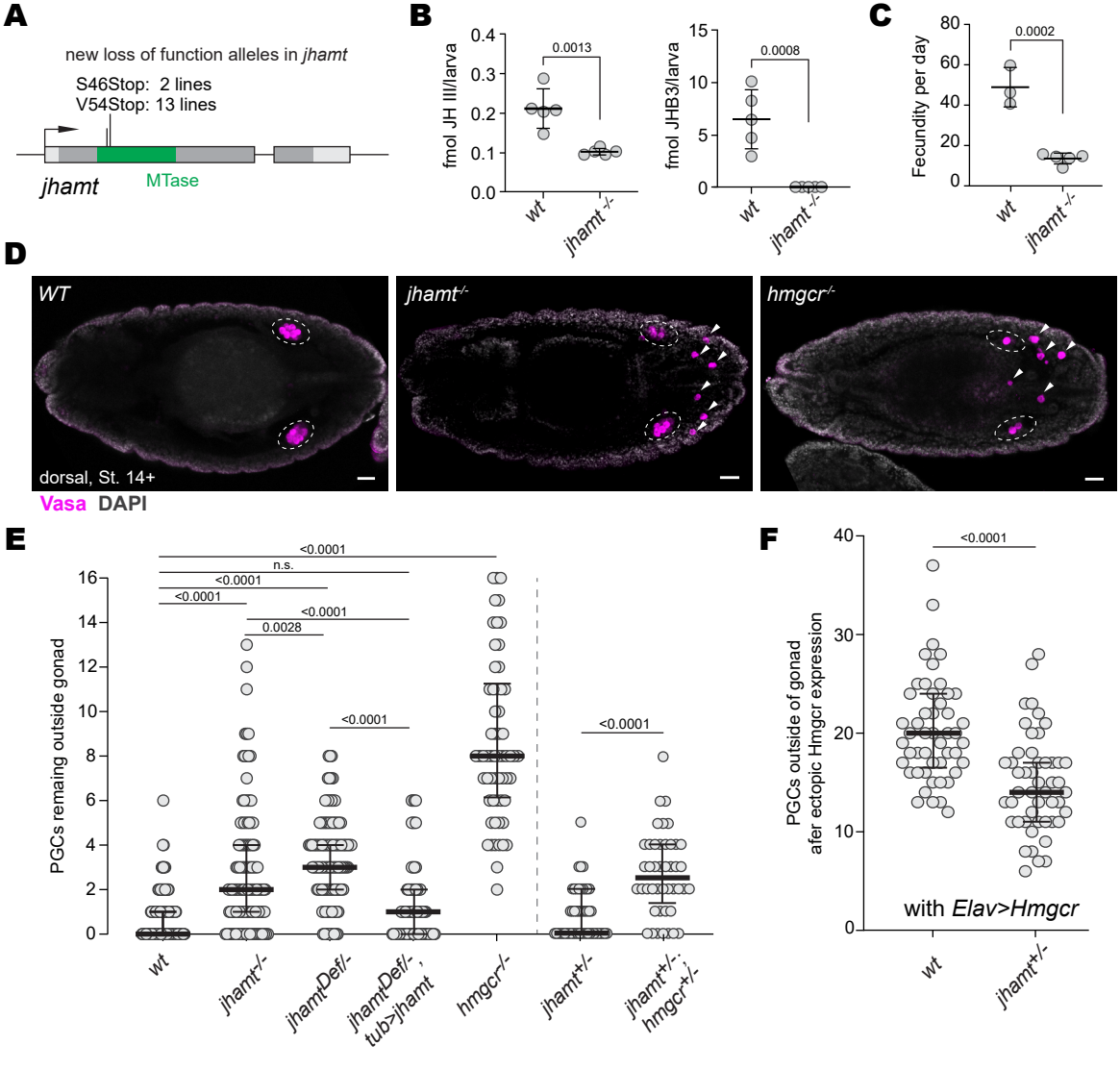

Figure 3
Juvenile hormone is sufficient for PGC migration

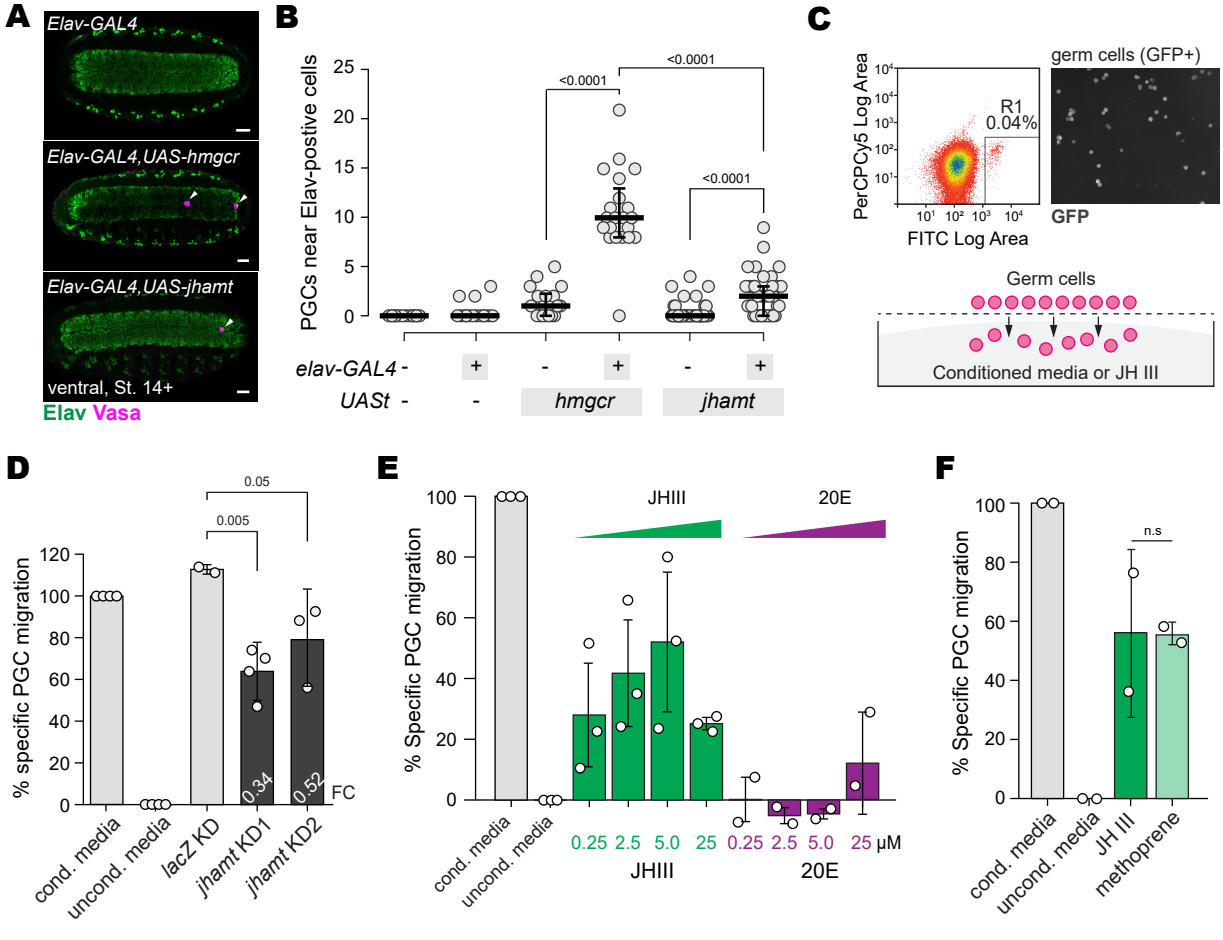

Figure 4
JH transcriptional receptor loss compromises PGC migration to the gonad

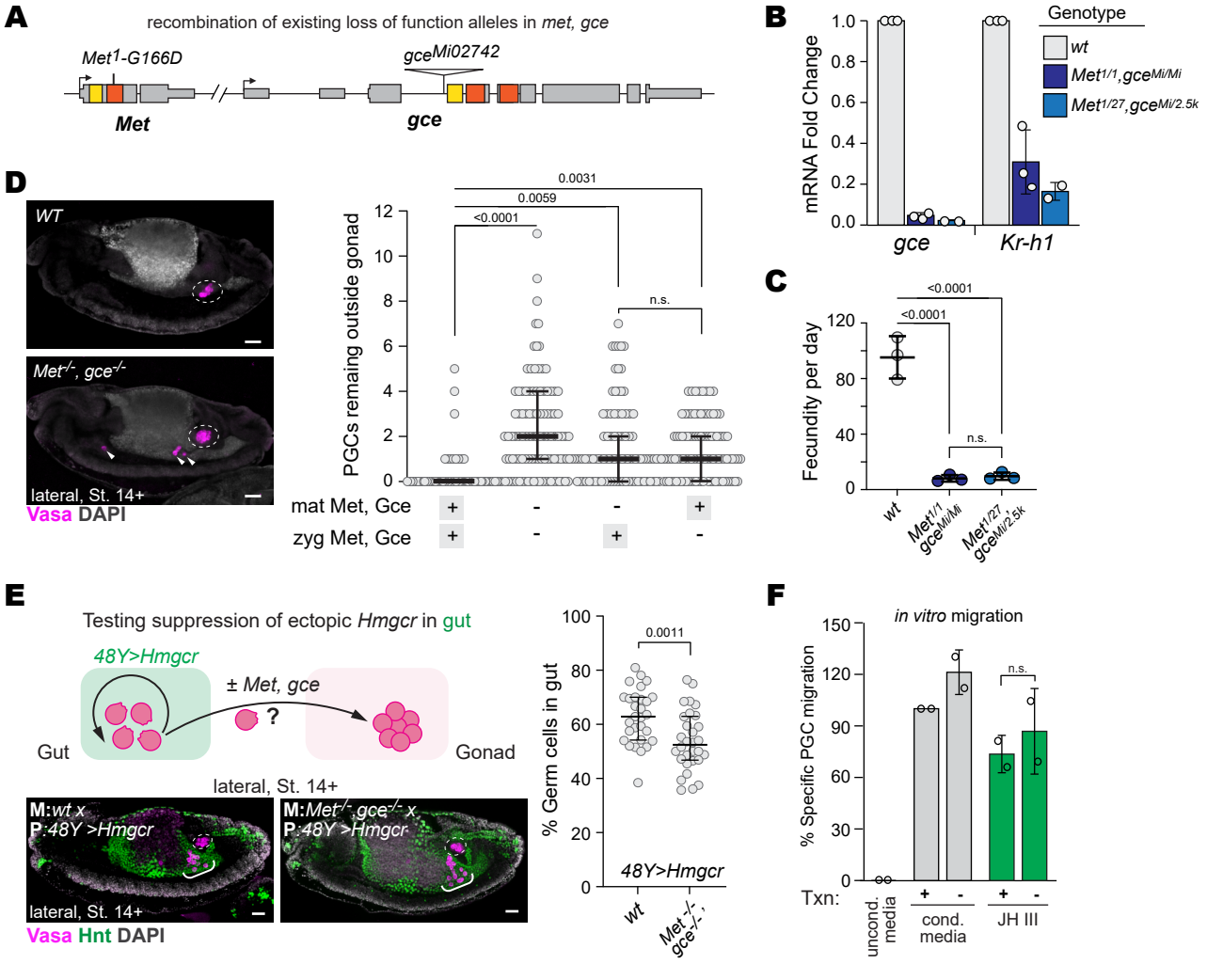

Figure 5
Compensatory feedback loop maintains JH homeostasis in *Drosophila*

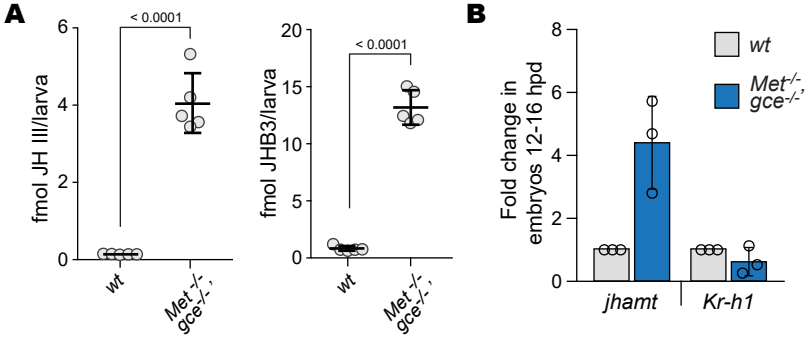

Figure 6
Model of JH function in PGC migration

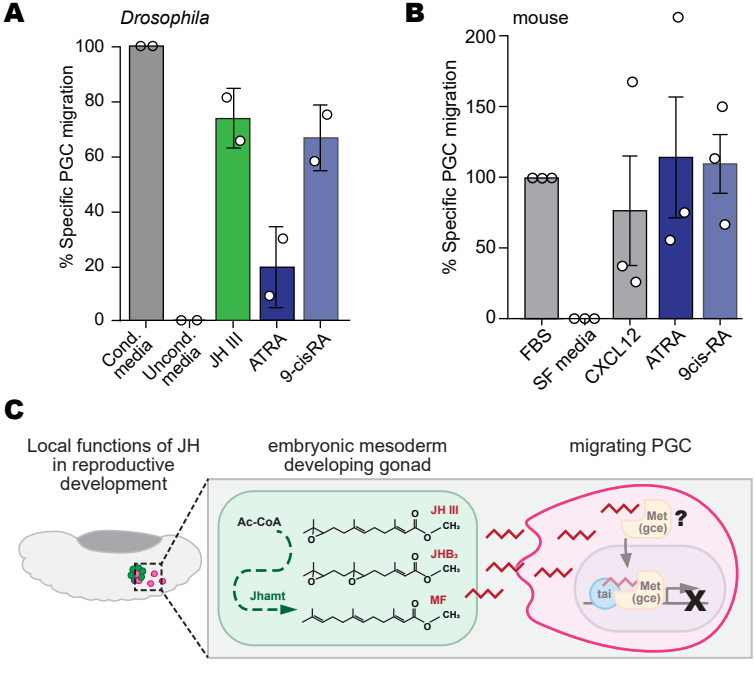

Supplementary Figure 1

A

```
JHRE Wt8x  -  5′ ccatcccaCACGCGaagacgataaaacca 3′
JHRE Mut8x -  5′ ccatcccaGTGCGCaagacgataaaacca 3′
```

B

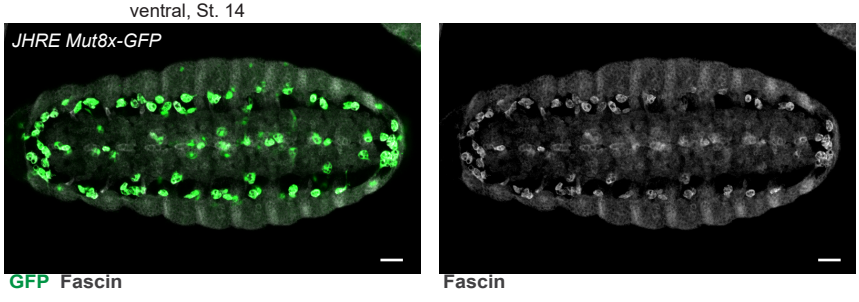

C

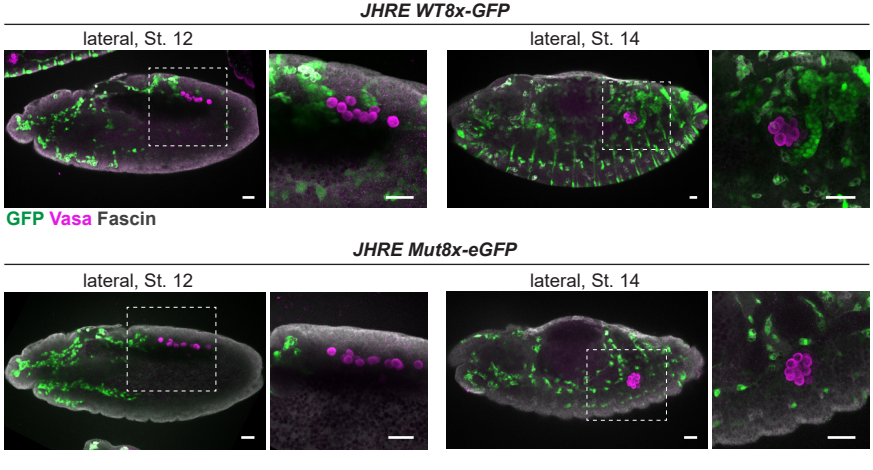

Supplementary Figure 2

Deletions in *jhamt* caused by guide: `CCTGGA|TGTGGGTTCAGGATCT`

Class I: frameshift leading to premature stop codon at a.a. 46

Lines with 5 bp deletion to generate `TC|TGT`: 12F1, 12F2

Class II: frameshift leading to premature stop codon at a.a. 54

Lines with `T` deletion to generate `GGA|GT`: 1F1, 1F2, 4F3, 6F2, 6F3, 7F2, 7F3, 8F1, 8F2, 12F3

Lines with `A` deletion to generate `GG|TGT`: 14M2, 14M3

Lines with `TCC` insertion and `G` deletion to generate `GGA|TTCCGT`: 4F1

Supplementary Figure 3

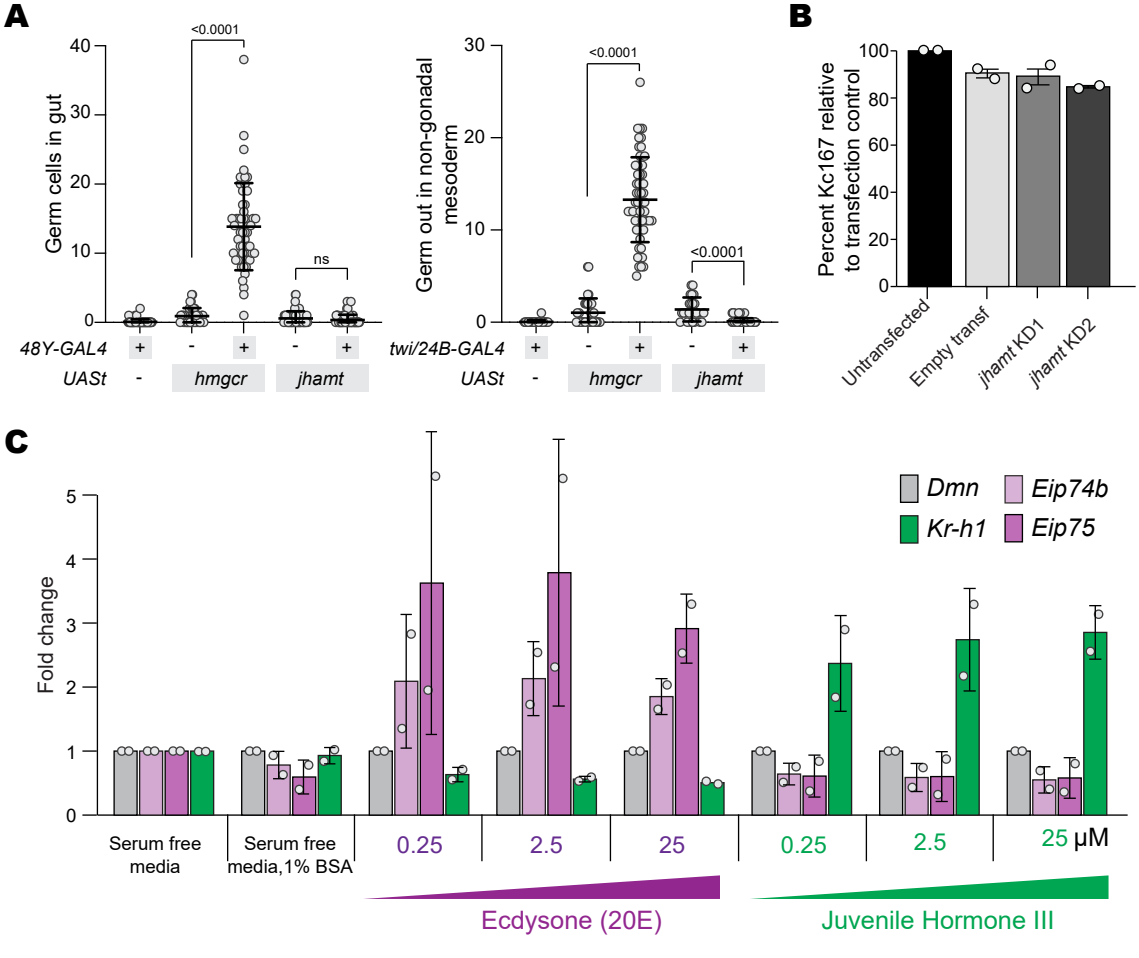

Supplementary Figure 4

A

Untreated PGCs

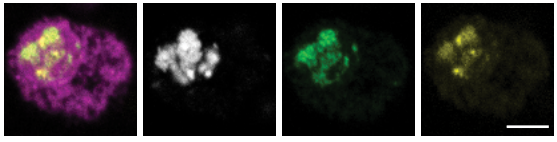

Flavopiridol treated PGCs

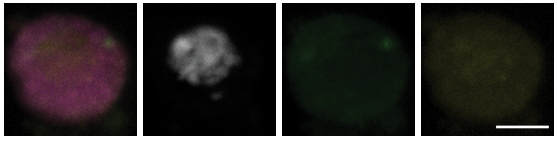

Vasa Merge **DAPI** **PolII Ser5** **PolII Ser2**

Supplementary Figure 5

A

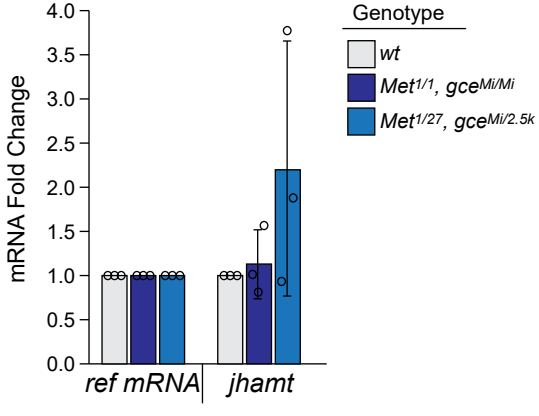

B

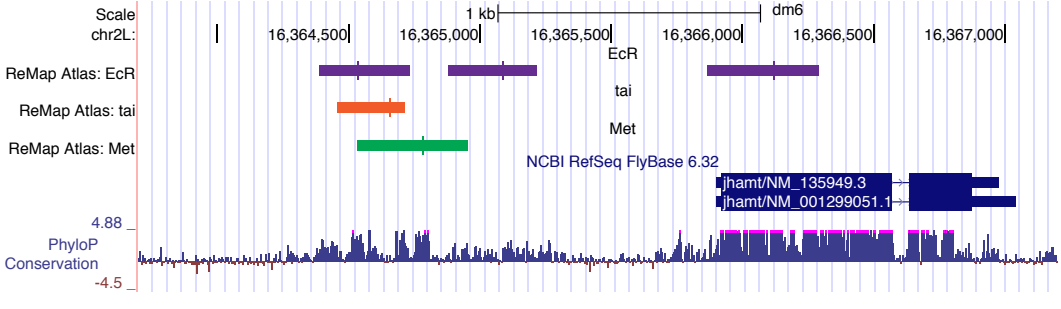
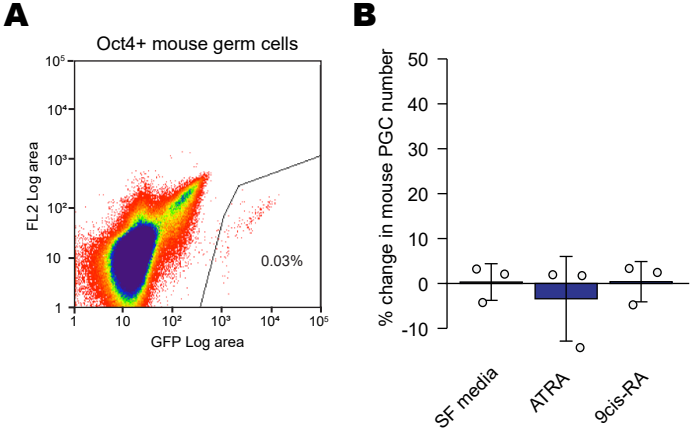
Supplementary Figure 6